Chair of Physical Metallurgy

Master's Thesis

Towards new approaches for APT specimen preparation with fs-laser ablation

Christian Hofer, BSc

September 2024

MONTANUNIVERSITÄT LEOBEN
www.unileoben.ac.at

EIDESSTATTLICHE ERKLÄRUNG

Ich erkläre an Eides statt, dass ich diese Arbeit selbstständig verfasst, andere als die angegebenen Quellen und Hilfsmittel nicht benutzt, den Einsatz von generativen Methoden und Modellen der künstlichen Intelligenz vollständig und wahrheitsgetreu ausgewiesen habe, und mich auch sonst keiner unerlaubten Hilfsmittel bedient habe.

Ich erkläre, dass ich den Satzungsteil „Gute wissenschaftliche Praxis“ der Montanuniversität Leoben gelesen, verstanden und befolgt habe.

Weiters erkläre ich, dass die elektronische und gedruckte Version der eingereichten wissenschaftlichen Abschlussarbeit formal und inhaltlich identisch sind.

Datum 14.09.2024

Unterschrift Verfasser/in
Christian Hofer

Acknowledgments

First of all, I would like to thank Prof. Ronald Schnitzer for the opportunity to write about this topic.

Thanks to Dr. Anna Jelinek for the supervision and for performing the focused ion beam preparation and proof of concept atom probe tomography measurements. Further thanks for the introduction into electropolishing and quality control of the electropolished specimens.

Also, I would like to thank Dr. Michael Tkadletz for the supervision and for the help using the fs-laser ablation system. Special thanks for the many ideas how to integrate the fs-laser into this work.

I would further like to thank Gerhard Hawranek for a variety of scanning electron microscopy investigations and for the help with the broad ion beam milling system.

Content

1 Introduction

Atom probe tomography (APT) enables three-dimensional compositional imaging with high analytic sensitivity at the atomic scale and is based on the principle of field evaporation of a sharp specimen apex [1,2]. The specimens have the special property that they are the image forming “lens” for the measurement itself [3], and strongly influence the electric field necessary for field evaporation [1,4]. Therefore, preparation techniques to reach a sharp needle shape with a radius of the specimen apex in the order of 10 up to 150 nm and an appropriate shank angle are of great interest [1,4].

Commonly used methods are either two-staged electropolishing or a focused ion beam (FIB) lift-out combined with annular milling sharpening processes [4–6]. Electropolishing is fast and does not require expensive equipment but is limited to conductive materials and the results are variable due to possible preferential etching of e.g. precipitations in high alloyed metals [7–9]. FIB methods are more accurate in producing a uniform circular cross-section and specific regions of interest (ROI) can be selected due to simultaneous scanning electron microscopy (SEM) imaging. Such dual-beam FIB/SEM systems have the disadvantages, that the lift-out process takes considerable amount of time leading to a bottle-neck due to machine workload and furthermore require a high operator’s skill level [4,6,10].

Following the recent progress in laser ablation systems finally resulting in femtosecond (fs)-laser ablation systems [11–13], the idea came up to further implement fs-laser processing in the preparation route of APT specimens. In order to secure comparability, for all experiments the same base material, 99.5 % pure iron, was used. Firstly, fs-laser ablation was used to substitute common low-speed precision saw or wire machining processes [4] to cut blanks in typical matchstick shapes or even to directly cut out improved geometries. Secondly, different laser beam directions of incidence of a fs-laser ablation system equipped with a translation stage were used to decrease the radii of the specimen apexes. Variations of the laser power and position of the laser focus spot further improved the outcome. Experiments with a rotation stage concluded this part. The resulting specimens were investigated by SEM and subsequently finalized for APT measurements via three different techniques: electropolishing, FIB annular milling and broad Ar^+ ion beam milling. The latter one was previously reported to be perfectly suitable for cleaning of APT specimens from hydrocarbon contamination using a similar system, while keeping the desired radius of the specimen apex and shank angle [14]. Finally, after more SEM investigations, proof of concept measurements of the three main preparation routes using a local electron atom probe tomography (LEAP) system were conducted.

2 Theoretical background

2.1 Atom probe tomography

2.1.1 Local electrode atom probe

APT evolved from field ion microscopy in 1967, when E.W. Müller first included a time-of-flight (TOF) mass spectrometer to develop a one-dimensional atom probe microscope [15]. Since then, the system was adapted and improved to the currently used state-of-the-art three-dimensional LEAP [16], which will be explained in more detail. Applying a high voltage V (2-10 kV) on a very sharp radius of curvature of the specimen apex r (<150 nm) results in an appropriate electric field F in the order of 10^{10} V/m, which is necessary for field evaporation of the atoms. Hereby, an additional term must also be considered, the field factor k_f, which describes the shape of the specimen apex and its electrostatic environment [1,4], according to Eq. 1:

$$F = \frac{V}{k_f r}. \tag{1}$$

A simplified setup of an atom probe is depicted in Fig. 1a including a specimen mount, a counter electrode with an aperture (approx. 40 µm in a LEAP) and a detector. Fig. 1b shows the name-giving component of a LEAP, the local electrode, a hollow cone shaped electrode, which enhances the electric field twice as much compared to a conventional counter electrode with a larger aperture [6,17].

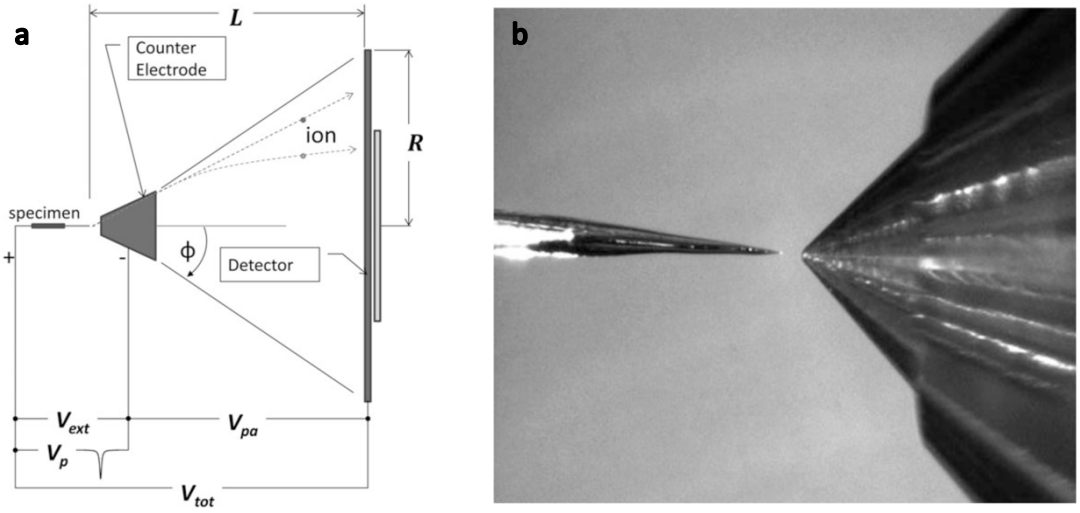

Fig. 1: (a) Schematic of an atom probe and (b) image of a local electrode with a 40 µm aperture at the apex and an aligned needle-shaped specimen in the LEAP [6].

Besides a constantly applied extraction voltage V_{ext}, either voltage pulses V_p or thermal pulses through laser irradiation are used to exceed the necessary field for evaporating atoms. Voltage pulsing is used for materials with high electrical conductivity

($S>10^2$ V/m, such as metals or heavily doped semiconductors), by applying pulses with an amplitude of 15-20 % of V_{ext}, either with positive polarity to the specimen or negative polarity to the counter electrode. The evaporation probability is kept relatively low (approx. 1%). Both, to avoid multiple simultaneous hits on the detector, which could otherwise lead to difficulties for position-sensitive detectors and to reduce the field-induced stress on the specimen [6]. Hereby pulse repetition rates are in the order of some hundred kHz [16]. In the case of many crystalline metallic materials, such as the investigated iron, the electrical field penetration is below 10^{-10} m, mainly affecting the atoms at the very surface of the specimen. So, evaporation takes place almost atom by atom and atomic-layer after atomic-layer [4]. While the electric field drags away such an atom, which leads to desorption, one/some of its electrons is/are drained to the surface, ionizing the atom [4]. Subsequently, the generated ions travel the flight path length L guided by V_{ext} to the (circular od risk shaped) detector with radius R (see Fig. 1a). Besides a hardware-wise given travel distance, the flight time is measured. This TOF mass spectrometry can distinguish between different mass-to-charge ratios [6]. All processes mentioned above occur within an ultra-high vacuum (UHV) system, with a pressure in the order of 10^{-11} mbar [2]. Furthermore, also a cryogenic cooling device for the specimen is needed to reach temperatures of 20-50 K in order to minimize surface diffusion [4,6].

2.1.2 Specimen requirements

The atom probe measurement principle demands strict limits for the specimen. Firstly, the radius r of curvature at the specimen apex, as schematically shown as red circle in Fig. 2, should be in the order of some 10 up to 150 nm. According to Eq. (1), a larger radius would require a too high starting voltage to start the evaporation process and the voltage limit of the LEAP with approx. 10 kV would be reached too early. The cross-section of the apex should further be circular to avoid artefacts in atom probe data reconstruction [4,18,19]. Secondly, the specimen must have a certain degree of robustness to withstand the pulsing and enough evaporation events (some ten millions) for the measurement [6]. Therefore, the surface should be free from protrusions, grooves and cracks [4]. But also, the shank angle α plays a significant role. Usually, a sharp needle with a modest semi-angle below 10° as depicted in Fig. 2 is favourable. A higher shank angle, e.g. a cusp shape has more mechanical stability and the electrical resistance is reduced due to a larger cross-section [16]. Whereas a smaller shank angle offers a slower increase in apex radius while probing, which can improve the data resolution in voltage pulsing mode [4]. Additionally, it has been found

that the field factor k_f from Eq. (1) does decrease with smaller shank angle [20,21]. Furthermore, the region of interest should be present near the apex. Regions, more than 100 nm away from the specimen apex may not be included within the dataset. Finally, the specimen should offer sufficient length itself to prevent shielding from the support structure and should be free from secondary apexes within 100 µm (as a conservative estimate) from the main apex. For apexes close to the specimen shank, this value can be reduced to 50 µm or slightly below in voltage mode. In laser pulsed mode this distance can be further reduced [4,6].

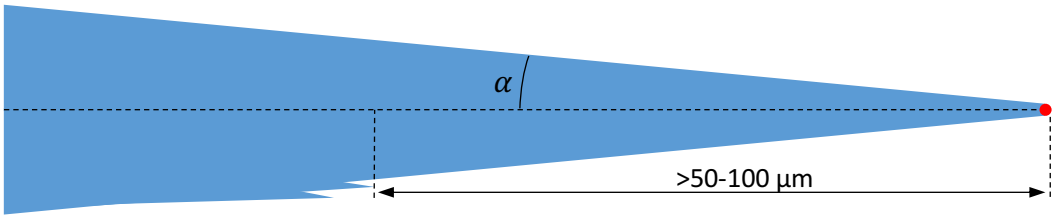

Fig. 2: Schematic of an APT specimen with a semi-angle α=5° and a red circle at the specimen main apex with a radius of curvature r. Secondary apexes are in sufficient distance from the main apex, according to a conservative estimate [4].

2.2 Conventional specimen preparation for atom probe tomography

2.2.1 Electropolishing

The first and more conventional one of the two main methods to prepare APT specimens is the two-staged electropolishing process, a step 1 rough polishing and a step 2 micropolishing. If no site-specific feature of the material, such as grain boundaries, should be investigated and the material is sufficient electrically conductive, this method is still an inexpensive and quite fast alternative to dual-beam FIB preparation [4,6]. The main material property requirement is high electrical conductivity to construct an electrochemical cell by applying direct current (DC), with the specimen set as anode and a grounded counter cathode, usually a noble metal wire, such as Au or Pt [2]. Alternate current (AC) is only used if a reactive layer is formed during polishing. Apart from the necessity of good conductivity, one other main disadvantage of the electropolishing method is possible preferential etching, especially at precipitates [7–9]. Fig. 3 shows a typical electropolishing curve, which in some cases might look slightly different depending on the material, temperature, electrolyte and geometry, but always shows the current between anode and cathode plotted against the voltage [4]. In this curve, the optimal condition for electropolishing is the plateau between the points B-C, where a µm thick viscous film with high ion concentration is responsible for smoothening the surface during polishing. The other two regions are

not favourable, between A-B preferentially etching of more reactive points takes place, whereas in region C-D the high current density and the resulting high hydrogen gas development disrupts the viscous film, which leads to pitting on the surface [2].

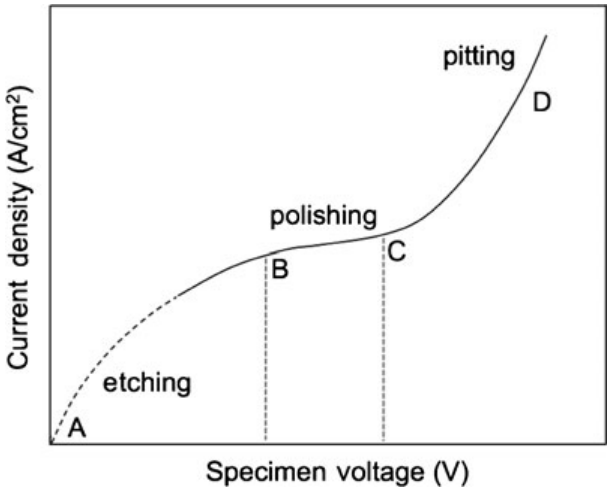

Fig. 3: Electropolishing curve with the three main areas etching (A-B), polishing (B-C) and pitting (C-D) [4].

Before starting the actual electropolishing process, the specimens should have a typical matchstick-shape, with 15-25 mm length and a square cross-section (e.g. 0.3x0.3 mm^2) or wires with a circular cross-section. This step is conventionally prepared by cutting of the bulk material with a low-speed precision saw or wire machining [4]. After this pre-preparation, the first electropolishing step, the rough polishing is traditionally performed according to Fig. 4a, but may vary depending on the lab setup.

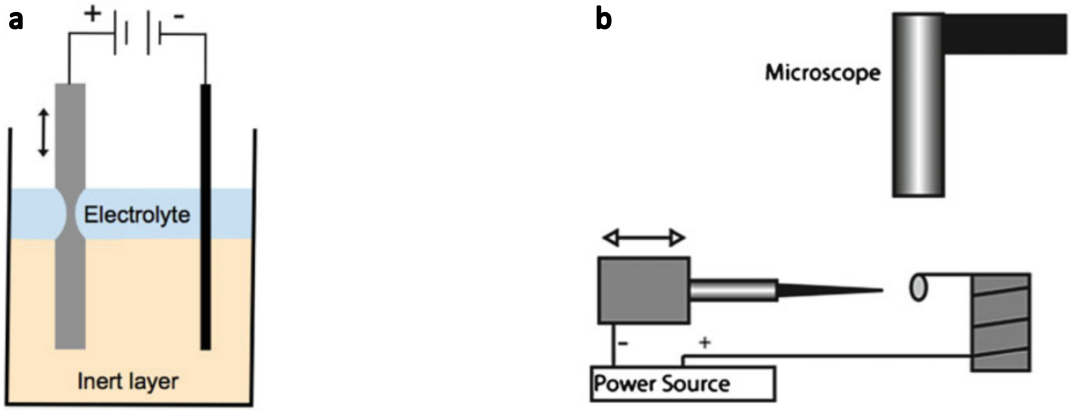

Fig. 4: Schematics of the two-staged experimental setup of the electropolishing process, with (a) step 1 rough polishing and (b) step 2 micropolishing [4].

The electrolyte layer, marked as blue, should be as thin as possible, but must be a continuous top layer. The optional inert layer below (e.g. Galden® perfluorinated ether heat transfer fluid), marked as orange, is used to reduce the amount of electrolyte

needed, and protects the lower part of the matchstick [6]. While applying DC or AC voltage, the specimen is moved up and down to control the shape of the necked region and avoid preferential attack at the air-electrolyte interface [2]. When the specimen breaks into two halves or the diameter is sufficiently lowered, the process is finished [4]. After cleaning the specimen, micropolishing is performed, usually with an experimental setup as shown in Fig. 4b. Hereby, a drop of a different electrolyte is suspended in a noble wire loop and frequently replaced due to rapid pollution of the small electrolyte volume [2]. While being moved forward and backward and giving voltage pulses, a necked region is formed on the right-hand side of the loop. With the aid of an optical microscope the moment just before breaking is identified and the specimen is moved backwards through the loop and the necked region is cut with short voltage pulses on the left-hand side of the loop. Finally, the specimen should be cleaned once more [6].

2.2.2 Focused ion beam

In contrast to the electropolishing process, dual-beam FIB methods do not use matchstick-shape precursor material, but the specimen is excavated out of the bulk surface with the in-situ lift-out process [6]. This first step starts with deposition of a protective layer over the ROI, as depicted by a green Pt bar in Fig. 5a. This layer is usually 2 µm wide with a thickness of around 20-100 nm and will later on protect the ROI from the Ga^+ ions, which are used for material removal. Fig. 5a further shows milling tranches at a cut angle of 30° to the surface normal [22]. They represent the orange doted lines in Fig. 5b on three sides of the bar of the material that is removed. This part is often referred to as wedge [4].

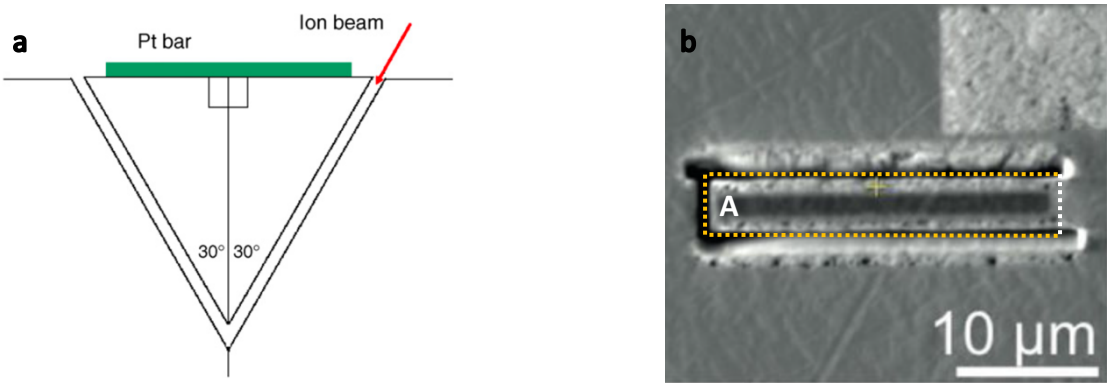

Fig. 5: (a) Schematic of the FIB lift-out cross-section [22] and (b) an image of the wedge directly before the micromanipulator is attached, adapted from [4].

Subsequently, a micromanipulator is attached on the left-hand side to point A of the wedge and a cut (white dotted line) at the right-hand side of the wedge is performed

[4,22]. The micromanipulator is used to move and attach the wedge on the support structure with a FIB deposited weld, as shown in Fig. 6a. A final cut, visualized by a white dotted line, concludes the lift-out process resulting in Fig. 6b [4].

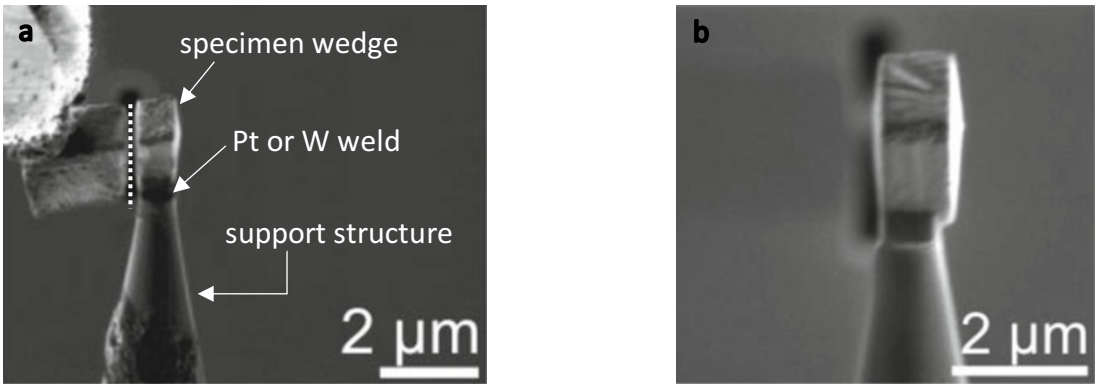

Fig. 6: Images of the specimen wedge and the support structure (a) before and (b) after the final cut in the FIB lift-out process, adapted from [4].

In order to fulfil the APT specimen requirements, subsequently a sharpening process, which include annular milling steps and a low-energy FIB clean-up step, must be conducted [6]. An annular milling pattern is applied on a specimen on a support structure (similar to Fig. 6b) to get the required specimen shape. To this end, the inner diameter and the ion current are progressively decreased during milling. The outer diameter used to be kept constant to avoid fluctuations of the centre alignment of the pattern [22,23], but can also be progressively decreased [11,16]. Finally, a low-energy (2 or 5 keV) step with a circular pattern that images the specimen end-on is performed to remove the damaged regions from the previous steps, performed at 30 keV [6]. The specimen end diameter is slightly smaller than the final inner pattern (if used), due to beam spreading [23]. But a final inner pattern can also be omitted, and a broad beam used instead [10].

2.3 Laser ablation systems

Due to the recent progress in development of laser ablation systems enabling the preparation of complex geometries in a reasonable time, several groups introduced either picosecond (ps)-laser or fs-laser ablation systems as a pre-preparation method for APT specimens [12,24–26]. Hereby, ps and fs stand for the range of the pulse lengths of the laser beam. Shorter pulse times (towards fs) are favourable, they reduce the thermal damage and the heat-affected zone (HAZ) of the material. A bigger part of the phonon excitation due to the electromagnetic wave from the laser is absorbed by

the electronic system of the material. The HAZ, if present, can be in the order of µm, depending on the material and laser parameters [13,27–29], is entirely removed during the subsequent sharpening process, e.g. using standard annular FIB milling [12]. In this work the effect of the thermal damage (and a HAZ) of the specimens will be neglected, due to the usage of an advanced fs-laser ablation system with a pulse length of 238 fs, as previously used by Tkadletz et al. [11]. One of the major advantages of such laser ablation systems is that the material removal is much higher than in plasma FIB systems [29], which themselves offer higher processing rates than Ga^+ FIB systems [30]. A demonstration of the preparation speed of a laser ablation system is depicted in Fig. 7a [12]. Examples of how laser ablation systems have already been incorporated into the APT specimen preparation process are discussed below. The main aim of the groups was to substitute the time-consuming FIB lift-out process.

First work was conducted by Rottwinkel et al. [12], who prepared transmission electron microscopy (TEM) specimens and APT specimens by ps-laser machining. The latter one, an array of specimen apexes, is shown in Fig. 7b as an example of free-form possibilities [12]. Heller et al. [26] investigated Hf-Si-B_2 thin films deposited on a Si wafer and used a ps-laser ablation system to directly mill APT posts, as shown in Fig. 7c, into the wafer. The specimens were finished with FIB sharpening. While reducing the time for the preparation process, the ROI (the Hf-Si-B_2 thin film) was not affected and successfully measured in APT to study the cluster behaviour of Si [26].

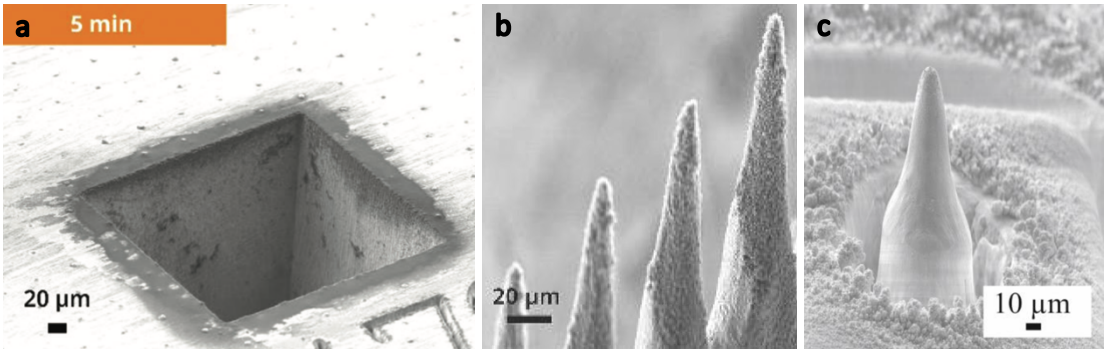

Fig. 7: (a) Visualization of the ps-laser preparation speed by milling a box (300x300x250 µm³) into Si within 5 min, (b) SEM image of Si APT specimens, adapted from [12], and (c) a specimen post after ps-laser ablation [26].

Another part of the APT specimen preparation which can be performed using laser ablation systems is the fabrication of microtip coupons. A single microtip is a specimen mount comparable to the support structure, previously shown in Fig. 6a, where the specimen can be welded on top after the FIB lift-out process. Several microtips are arranged in an array. Tkadletz et al. [11] prepared microtip coupons with fs-laser

processing directly on the sample of a TiN coated Si substrate and they performed equally well in LEAP measurements as regular commercially available coupons. Such an array of microtips, imaged directly after the fs-laser pre-preparation is shown in Fig. 8a. After imaging, the coupons were sharpened with FIB annular milling [11].

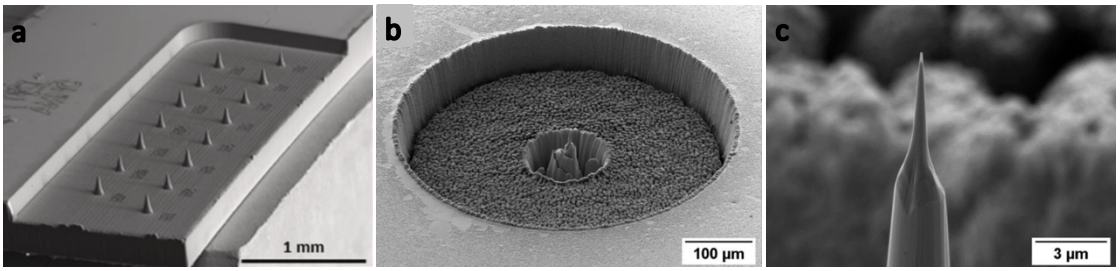

Fig. 8: (a) Backscattered image of a fs-laser prepared APT Si microtip coupon [11]*, (b) and (c) SEM images of a fs-laser ablated crater into an Inconel® alloy with a Ga^+ ion milling finish for the APT specimen* [25].

Apart from studies investigating Si as base material or thin films, also the pre-preparation of metallic materials was performed. Tkadletz et al. further successfully processed microtip coupons into different materials using a fs-laser ablation system, such as Al, Ti, Fe, Co, Ni, Cu, Mo, W and WC-Co, supplementary material for [11]. Hestad et al. [25] substituted the lift-out process for an Inconel® specimen by fs-laser ablating a crater into the bulk material, similar to the FIB moat method [23]. Subsequently the specimen was sharpened with Ga^+ ion milling and successfully measured in a LEAP. The final shape is depicted as overview SEM image in Fig. 8b and with higher magnification in Fig. 8c [25].

2.4 Broad ion beam milling

Another preparation technique that has been implemented in APT related topics is broad ion beam (BIB) milling. Hereby, a broad beam (in the order of a few mm) of Ar^+ ions is used instead of the more focused beam of Ga^+ ions in a FIB [31]. Because this process is also ideally significantly less material selective, it is used as a final step for even material removal to (re-)shape APT (or similarly shaped field emitter) specimens [8,9,14,31]. Firstly, the (re-)sharpening of blunt field emitter specimens shall be discussed. Walls et al. [9] sharpened blunt or pre-etched Ir specimens with a radius at the specimen apex of around 1 µm using Ar^+ ions with an acceleration voltage of 6 kV and a beam angle perpendicular to the axis of the rotating (5 rpm) specimen. After 1 h the emitter apex radius was reduced to 200 nm with an appropriate shank angle and

after 2 h the specimen was sufficiently sharp for low voltage field-ion measurements. In this case, electropolishing was not even an alternative due to the formation of heavily contaminated surface of Ir during polishing [9]. Since the invention of atom-probe field-ion microscopy, several groups suggested ion milling processes for this purpose. Here, a useful case for broad ion beam milling is the investigation of multi-phase alloys, such as WC-Co, which are susceptible to selective etching during the electropolishing process. To remove small amounts of material of pre-shaped WC-Co specimens and securely reach the ROI while maintaining a needle shape, Henjered et al. used 4 kV Ar^+ broad ion beam milling (25 nm/min) steps with TEM control in between [8]. While the previously mentioned studies used an ion beam direction perpendicular to the specimen axis, Larson et al. [31] investigated the influence of variations of the milling angle β between 0° and 35°, as shown in Fig. 9a. For the ion milling, 3 keV Ar^+ ions, a rotating specimen, and a beam diameter at the specimen of approximately 3 mm was used. In the following only the two extreme values β = 0° and β = 35° shall be discussed briefly. If β = 0°, the material removal from the near-apex region is higher than along the shank, resulting in an arrowhead shape. Whereas a β of 35° leads to stronger material removal from the shank region due to physically blocking of the specimen apex by the specimen shank [31].

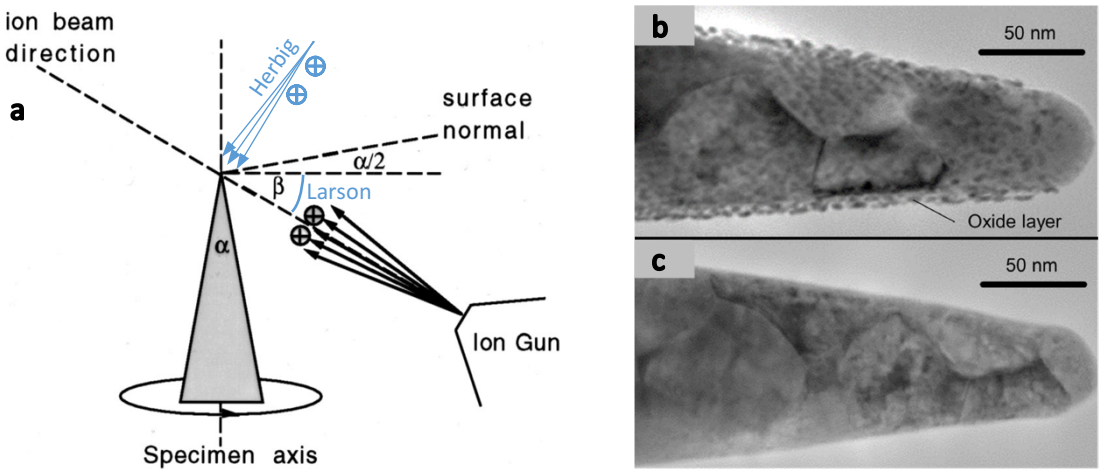

Fig. 9: (a) Schematic of broad Ar^+ ion beam angle variations, adapted from [31], *(b) different experimental setup with TEM images of an oxidized and hydrocarbon-contaminated APT specimen before and (c) after BIB milling, adapted from* [14].

Another different approach to use BIB milling as an addition to the APT specimen preparation process was performed by Herbig and Kumar [14]. They tried to improve the specimen yield, by removing oxide films and hydrocarbon contamination from APT

specimens out of steel with 2 kV Ar^+ ion cleaning. The experimental setup was slightly different compared to Larson et al. [31] in Fig. 9a. The Ar^+ ion beam angle was 35° tilted to the specimen axis measured top-down, corresponding to a β of -55°. Furthermore, the APT specimens were mounted in grid holders. With a specimen rotation around its axis of 25 rpm the 8 nm thick contamination layer was evenly removed from all specimen sites within 5 min. This progress is depicted in Fig. 9b with a thin contamination layer and in Fig. 9c after cleaning, which lead to a smooth APT voltage curve without any fracture events during the APT measurement [14].

These results are consistent with those of Sato et al. [32] investigating low energy Ar^+ ion preparation of TEM lamella. Due to the broader beam around 1 kV compared to the Ga^+ FIB, while still offering sufficient probe current, uniformly milling of the lamella with 0.5-2 kV Ar^+ polishing was successfully performed. This process even led to higher quality TEM images with fewer artefacts than Ga^+ FIB finishing [32].

3 Experimental methods

All APT specimen pre-preparation steps were conducted with fs-laser ablation and finished differently, according to Fig. 10. The three main preparation routes were: fs-laser & electropolishing, fs-laser & BIB milling and fs-laser & FIB annular milling. The experiments were concluded with proof of concept APT measurements.

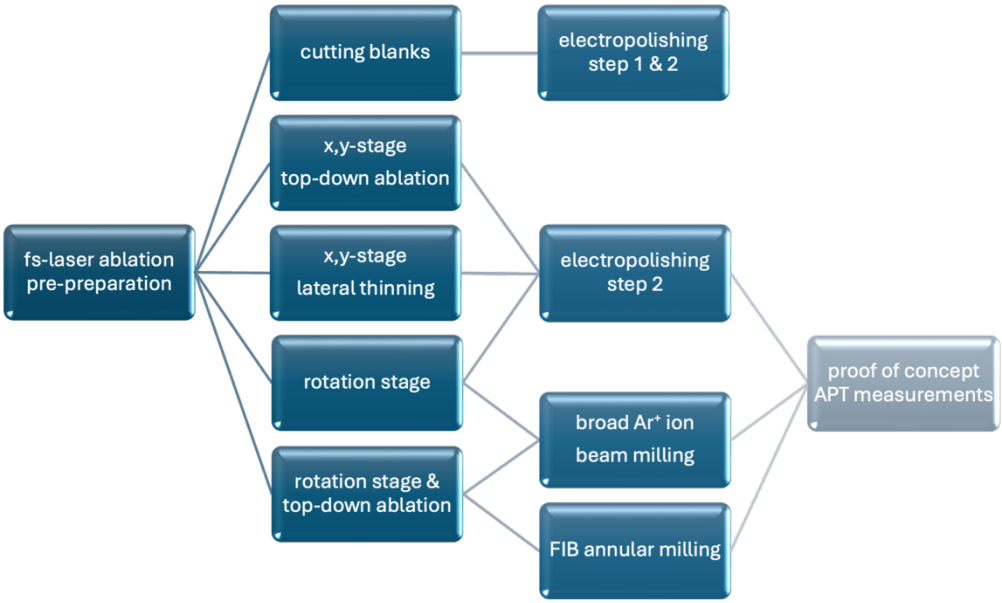

Fig. 10: Organization chart of the experimental routes for APT specimens in this work.

3.1 fs-laser ablation

For the whole fs-laser (pre-)preparation of this work 99.5 % pure Fe from HMW Hauner GmbH & Co. KG was used as base material, either as a 1 mm thick sheet or as rod with 2 mm diameter. The fs-laser ablation processes were conducted with a 3D-Micromac microPREP PRO FEMTO laser micromachining system using a wavelength of 532 nm. Due to previously conducted work by Tkadletz et al. [11] the pulse length was set to 238 fs, with a frequency (repetition rate) of 60 kHz. Furthermore, the pulse distance and the line distance of the laser pattern were set to 3.00 µm and the vector scanning mode was bidirectional. The laser beam size was Gaussian distributed with 8 µm full width at half maximum (FWHM). All laser parameters mentioned above were kept the same during all experiments, the laser beam size could only be fictitiously changed for the pattern calculation, this parameter was called laser spot. Depending on the intended use and individual process step the laser power was varied between 50 mW and the maximum power of this system of 2.5 W. Due to the low penetration depth of the laser beam, the currently ablated part of the specimen would not always be in laser focus, if not corrected. These adjustments were reached by software-controlled

movement (z-axis) only of the respective stage. This movement will be referred to the term laser focus shift [µm] in the following and was processed within a certain number of so-called focus levels [-]. Whereas the focus position of the integrated cameras (overview and detail) and the laser focus position of the microPREP system were all fixed. The choice of the implementation of a laser focus shift, including focus offset (an initial single focus shift of a specific pattern area), a certain number of focus levels and a processing depth was chosen according to the used stage, pattern and the material thickness. If needed, the focus weakening itself was used to generate a field emitter-like specimen shape with an appropriate shank angle of the specimen. Furthermore, cleaning was performed using a CO_2 snowjet system (as standard cleaning) or compressed gas bottles (for apex radii in the low µm regime and below).

3.1.1 x,y-stage: Laser beam directions of incidence

In the following some further 3D-Micromac microPREP PRO FEMTO specific terms shall be introduced briefly. The translation stage will be from now on designated as x,y-stage and is partly shown (moveable disk) at the bottom side of Fig. 11a and b. The black dash-dotted lines mark the specimen axis. The convention for top-down ablation & thinning was laser beam parallel to the specimen axis (Fig. 11a) and for lateral thinning the laser beam was perpendicular to the specimen axis (Fig. 11b).

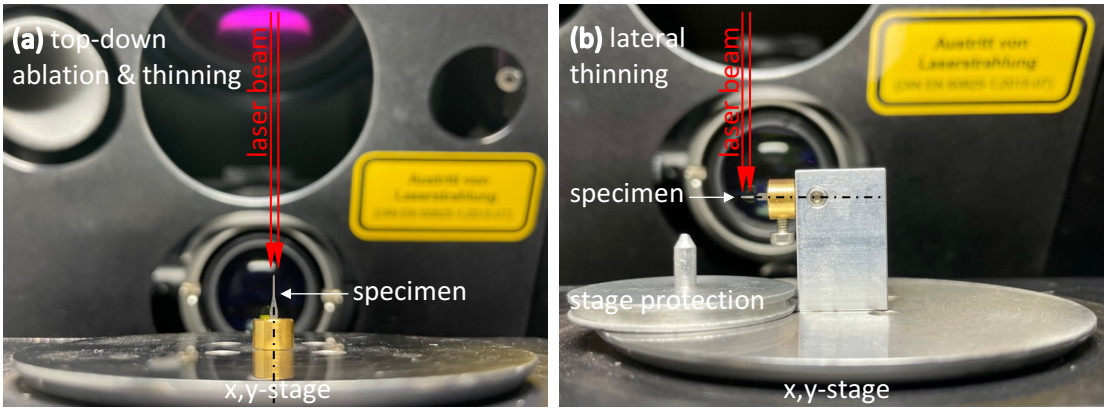

Fig. 11: Definition of 3D-Micromac microPREP PRO FEMTO specific terms concerning the directions of the incident laser beam, using the translation (x,y-)stage of (a) the top-down ablation & thinning and (b) the lateral thinning processes.

The lateral thinning processes had another special feature for the incident laser beam, the work angle. A small specimen tilt of ±5° against the laser beam direction of incidence was used to minimize the taper in cutting direction, as depicted in Fig. 12. So, a gradual width increase towards the backside of the blanks or specimens could be minimized, but not completely avoided.

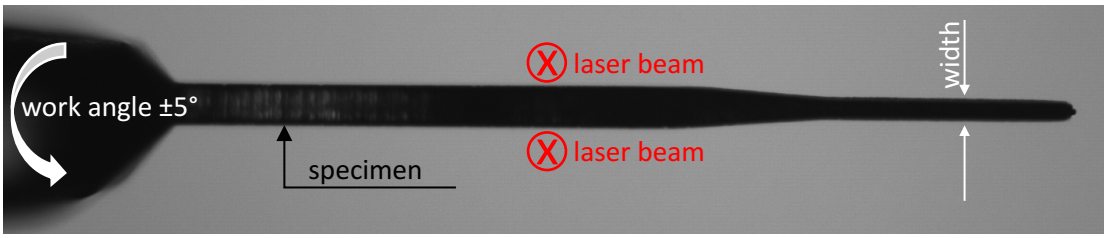

Fig. 12: Definition of the 3D-Micromac microPREP PRO FEMTO specific term "work angle" for pre-cutting of APT blanks and lateral thinning processes.

3.1.2 x,y-stage: pre-cutting of APT blanks

In order to fully ablate through the 1 mm thick Fe sheet following parameters were used: The maximum power of 2.5 W, 176 repetitions per layer with shifted layering scan regime, 20 µm laser focus spot and 1000 µm laser focus shift within 100 focus levels. Fig. 13 shows an optimized shape for an APT specimen blank with an apex size of 40 µm, but the principle is the same as cutting out rectangular or slightly tapered blanks, which were also prepared in this work. For the first layer a work angle of -5° was chosen and for the second layer +5°. All blanks had a length of 12.7-12.8 mm in common, resulting in similar process times per blank of 40-60 min. The (custom) shape of Fig. 13 was cut out blank per blank, whereas the standard rectangular and slightly tapered blanks were processed together in series of 10-20 pieces at once.

Fig. 13: Two-layered custom shape for cutting out optimized APT blanks with a fs-laser.

3.1.3 x,y-stage: top-down ablation and thinning

For this purpose, mainly the standard fs-laser pre-prepared rectangular blanks were fixed in a brass FIB/SEM single holder with a 2 mm hole and a clamping screw. Subsequently, top-down ablation or thinning of the 1x1 mm^2 cross-section, visualized as blue areas in Fig. 14a-d, was performed. The black lines mark the laser patterns. While the outer pattern of the top-down ablation processes, as shown in Fig. 14a-c, remained the same at 1.25x1.25 mm^2, the inner pattern was varied. Ablation parameters of Fig. 14a-c were shifted layering and 20 µm focus spot within a single step with 2.5 W power, 350-501 repetitions, 0-750 µm focus shift and 100 focus levels. The first experimental series were circle ablation with a starting diameter of the inner circle in Fig. 14a of 200 µm for the first specimen and stepwise reduction down to

20 µm. Whereas the pattern in Fig. 14b, with a bigger inner circle of 250-500 µm, was used just to remove secondary apexes and represents an optional extra step. For comparison, also square ablation experiments were performed, with a pattern geometry according to Fig. 14c and inner squares with 100x100 µm² and 200x200 µm².

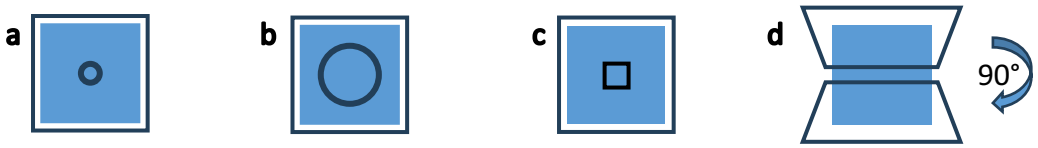

Fig. 14: fs-laser patterns of top-down (a) circle ablation, (b) removal of secondary apexes, (c) square ablation and (d) thinning including a manual 90° specimen rotation.

All processes mentioned above, including the optional removal of secondary apexes, lasted about 24-42 min in total. To explore further possibilities of the fs-laser system, also top-down thinning experiments were conducted. Hereby, the parameters were slightly different, with a diameter of the laser focus spot of 7 µm and rotated layering and a manual 90° specimen rotation between the two steps, as indicated in Fig. 14d. Also, the slightly tapered blanks, with a cross-section at the apex of 250x1000 µm² were used for this purpose. For pre-thinning these blanks to 250x250 µm², preparation of only the longer side was sufficient. The size of the trapezoid patterns was varied depending on the used blanks and the resulting cross-section after the 90° rotation. Preparation time reached up to 27 min for the standard blanks, using the tapered blanks lowered the time consumption to 8-18 min. The end contours of 50x50 µm² up to 70x70 µm² were reached with a power set to 2.5 W, without focus shift and 2x251 repetitions. Furthermore, combinations of top-down thinning followed by circle ablation were conducted. Therefore, circular patterns with 20 µm inner diameter were ablated within 2-4 min on 100x100 µm² up to 300x300 µm² pre-thinned specimen.

3.1.4 x,y-stage: lateral thinning

For this multi-step process the brass specimen holder was 90° tilted, in order to ablate the specimens with the laser beam perpendicular to the 12.7-12.8 mm long side of the rectangular or slightly tapered blanks, into the drawing plane of Fig. 15a-c. The blue coloured areas mark the specimens in shortened length (not in scale), whereas the trapezoid patterns are marked as black lines. All individual steps had in common a manual 90° rotation around the specimen axis at the preparation half time, a work angle of ±5°, an individual focus shift in the order of the processing thickness and the thinning parameters of 7 µm focus spot and rotated layering. The pre-thinning step (Fig. 15a) was performed using 2.5 W laser power with 2x55 repetitions and 100 µm

width of end contour. Hereby, the preparation time for the slightly tapered blanks was reduced for 1-2 minutes, due to the smaller pattern size that could be used for the shorter side (tapered from 1000 to 250 µm) of the specimen. Secondly, thinning to an end contour of 20-40 µm using 250 mW and 2x126 repetitions was performed according to Fig. 15b. Further optional processing with 100 mW to the minimum possible end contour of the fs-laser system of 1 µm is depicted in Fig. 15c. Total laser processing time required for this route was 18-27 min. Additional experiments after the first lateral thinning step to 100x100 µm^2 with subsequent top-down circle ablation with 20 µm inner pattern diameter, similar to section 3.1.3, were also conducted.

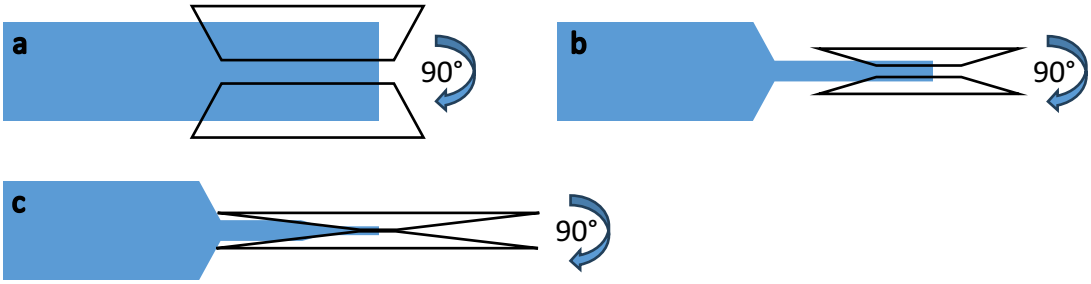

Fig. 15: Schematics of the trapezoid fs-laser lateral thinning patterns, with widths of the end contours of (a) 100 µm, (b) 20-40 µm and (c) 1 µm.

Another more sophisticated approach to directly generate specimens with an end contour width of 40 µm is shown in Fig. 16. Therefore, pre-cut blanks from Fig. 13 were used and the laser pattern choice was modified: instead of simple trapezoid patterns, individual patterns (custom shapes) were used. The work angle of layers 1,3 and 5 was -5° and of layers 2, 4 and 6 +5°. Concerning the area dose, for layers 1 and 2 the power was set to 2.5 W with 200 repetitions and for layers 3 and 4 to a lower power of 1 W with 70 repetitions. Layers 5 and 6 were optional and included a manual 90° rotation to gently recut the primarily shape of the blank with 500 mW and 100 repetitions. For all layers, pairwise (1 & 2, 3 & 4, 5 & 6) individual focus shifts or even offsets were used, depending on the starting focus position. Total process time was 14-21 min.

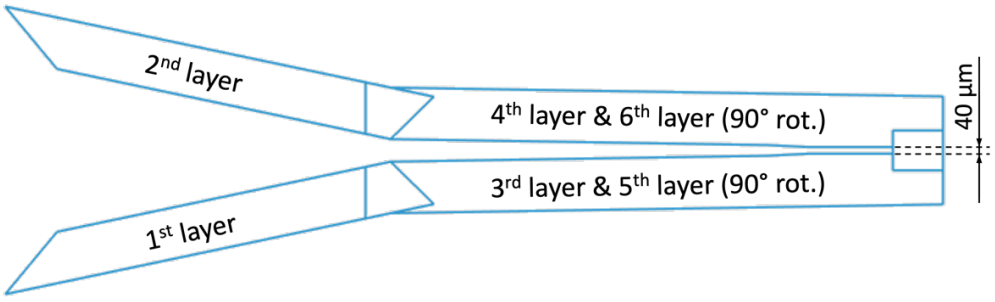

Fig. 16: Multi-layered custom shape for fs-laser ablation with layers 1-4 in a single process and layers 5 & 6 after a manual 90° specimen rotation.

3.1.5 Rotation stage

The rotation stage enabled automatised and software-controlled movement around the specimen axis, visualized as black dashed lines in Fig. 17a-e. In this way, the manual 90° specimen rotation was omitted, and other rotation angles were possible. The blue areas show again the specimens, which were either rectangular blanks or rods with a diameter of 2 mm. Laser ablation direction was perpendicular to the drawing plane, as in the previous section 3.1.4. Using the rotation stage required the determination of a centre of rotation, which was performed in the microPREP software. In order to not disturb the rotation centre, usage of a focus shift with the accompanying extra movement of the specimens was omitted (except for cutting). Another general laser parameter was shifted layering and 7 µm focus spot.

The first step, shown in Fig. 17a, and the optional removal of the edges, shown in Fig. 17c, were performed using 2.5 W power, 8-12 rotation steps of 20-30° with 40 repetitions per step. Due to the double-sided pattern achieving at least 180° rotation angle was sufficient to work around the rod. The width of the end contour at the bottom side of Fig. 17a was 120-150µm. If necessary, the centre of rotation was re-determined after this first step. To reach the final end contour width of 1-30 µm, as depicted in Fig. 17b and d, 1-2 processing steps with lower energies of 50-250 mW and 38-65 rotation steps of 3-5°, with 20-40 repetitions per step, were used. Furthermore, a single rod specimen was prepared with a semi-automatic single 90° rotation as a final step, comparable to section 3.1.4. Hereby, the power was set to 50 mW with 2x200 repetitions. Required total process time was around 60 min for the rectangular blanks and 80-90 min for the 2 mm circular rods.

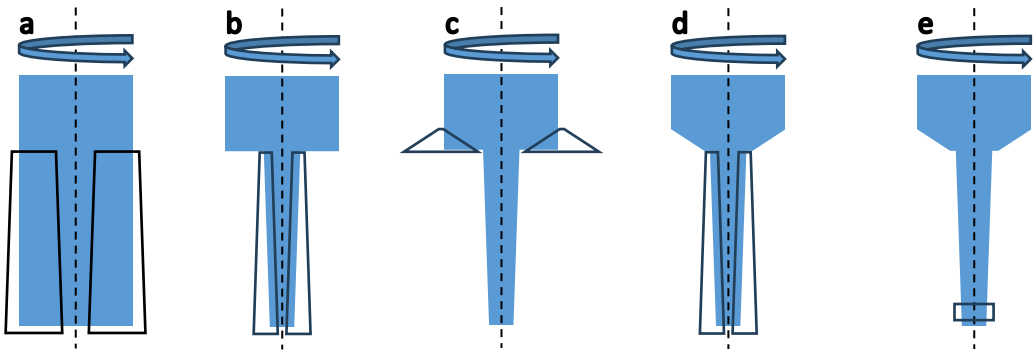

Fig. 17: fs-laser rotation stage patterns for (a) the general pre-shaping step, (b) the standard finishing process using lower energies, (c) an optional step to ease electropolishing, (d) the finishing process including preceding step c and (e) a rectangular box pattern for cutting, with a height of 200-300 µm and varying length.

Analogous to the previous sections, also experiments with subsequent top-down circle ablation were conducted. Therefore, either specimens after the first rotation stage step were used or existing ones were cut with the rotation stage and 50 mW to an end diameter of 60-100 µm. For the cut a similar approach with a box pattern (Fig. 17e) to that in the following paragraph was carried out, but in smaller dimensions. The final ablation inner circle diameter was varied between 4 and 20 µm, the laser power was set to 100 mW, with 1001-2001 repetitions and an optional focus shift of 200 µm within 50 focus levels.

Apart from preparing APT blanks, the rotation stage was also used to cut the Fe rods with 2 mm diameter into 12 ± 0.2 mm long pieces. Therefore, the build-in optical microscope of the laser ablation system and the micrometre screw turned out to be helpful. The laser parameters were set to 2.5 W for 16 steps of 45° with 24 repetitions each. Corresponding to a twice complete rotation of the specimen due to the single-sided rectangular box pattern of 250x2200 µm (analogous to Fig. 17e). Furthermore, a focus shift of 1000 µm within 8 levels was applied to optimize the cutting speed, ignoring negative effects on the centre of rotation. This led to process times of 11 min per cut.

3.2 Electropolishing

The only specimens used for electropolishing step 1 were the standard rectangular blanks with 1x1 mm^2 cross-section, for micropolishing step 2 also all other fs-laser pre-prepared shapes were used. This part was performed similarly to the standard electropolishing process previously described in section 2.2.1. Including one exception of the preparation technique, thinning of the specimen apex was performed without forming a necked region in step 1, as shown in Fig. 18a.

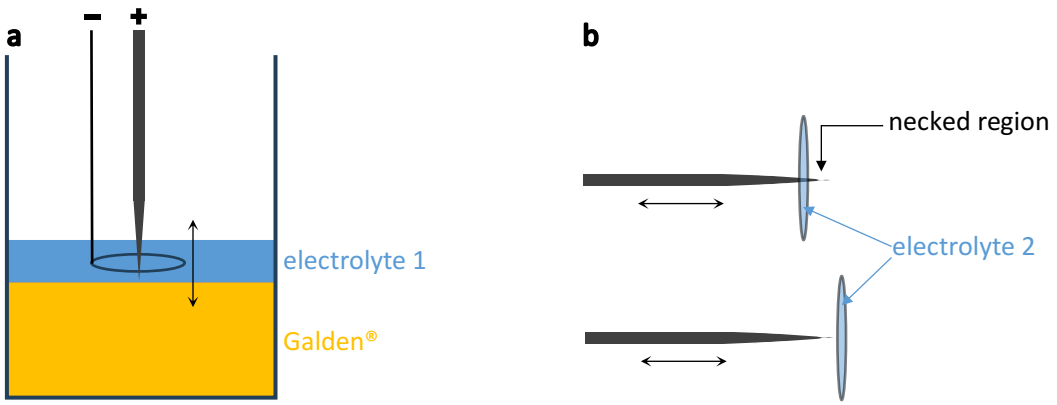

Fig. 18: Experimental setup of (a) electropolishing step 1 with electrolyte 1 on top of an inert layer (Galden®) and (b) micropolishing step 2 using a different electrolyte 2 only.

Furthermore, with a few exceptions, the usage of Cu sleeves, which often serve as specimen holder for smaller blank diameters, was generally omitted. Although not explicitly mentioned in the schematics in Fig. 18a and b, both steps were monitored through optical microscopes. As electrolyte 1 perchloric acid (25 vol%) in glacial acetic acid was used and as inert layer Galden®. The applied DC voltage in step 1 between Au loop and specimen was varied and stepwise reduced starting around 16 V and finishing around 11 V, leading to preparation times of 7-30 min. While the main preparation time was performed moving the specimens up and down within the loop, the final thinning was conducted slightly above the loop with reduced voltage. After reaching a sufficiently small end diameter of the specimen apex, the specimens were cleaned using distilled water, acetone and propan-2-ol. Subsequently, micropolishing step 2 was performed using 2 vol% perchloric acid in 2-butoxyethanol (electrolyte 2), which was placed inside an Au loop (Fig. 18b). Here, DC voltages of 8-12V between specimen and loop were applied, with decreasing voltage towards the end. The preparation time varied extremely between 1 and 15 min due to different starting diameters from the fs-laser pre-prepared specimen. Final cleaning was performed using propan-2-ol only.

3.3 Broad ion beam milling

For BIB milling 12 ± 0.2 mm long cylindrical Fe rods with a diameter of 2 mm were used as precursor material. The shape of those rods and the end diameter at the specimen apex of around 2-10 µm was pre-prepared as described in section 3.1.5, with the fs-laser and the rotation stage and optional subsequent top-down circle ablation. Tight tolerances concerning the specimen length were important in order to hit the apex with the Ar^+ ion beam. For this purpose, a turned Al adapter was used to adjust the height and centre the specimens in the standard holder of a Hitachi Ion Milling System ArBlade 5000 system. The specifications of the Al part, shown in Fig. 19a, were as following: a 50 mm outer diameter with a 7 mm deep and 44 mm wide mill-cut. On the bottom a 5 mm deep drill-hole with 2 mm diameter provided enough support for the specimen. So, the fragile fs-laser pre-prepared specimens could be placed into the drill-hole of the adapter after adjusting the holder position. Subsequently, the Ar^+ ion milling was performed in flat milling mode, with fast rotation (25 rpm) setting. While keeping the discharge voltage constant at 1.5 kV, the acceleration voltage was varied between 2 and 4 kV. Despite the broad ion beam, in some chases a slightly oscillation of the stage (0.5 turn adjustment) was used to be sure to hit the specimen. Weakening of the ion beam dose was compensated with an increase in preparation time, which was conducted in steps between 10 and 120 min. The designation of the milling angle β was equated to the tilt angle of the stage for the sake of simplicity and is visualized in

Fig. 19b. In the beginning, β was kept at 35°, while varying the other parameters. Later on, milling experiments with a β of 15° and 60° were conducted.

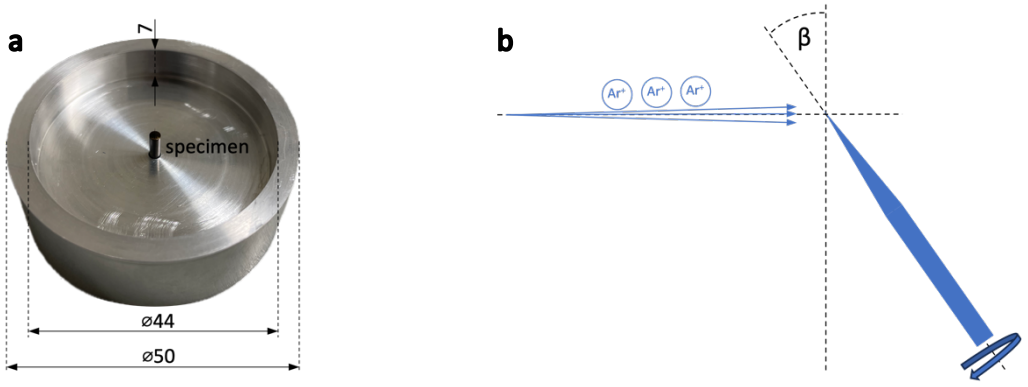

Fig. 19: (a) Turned Al adapter providing height adjustment and central fixation of the fs-laser pre-prepared specimens, all in [mm] and (b) schematic of the experimental arrangement of specimens and Ar^+ beam during the BIB milling process, with β = 35°.

3.4 Focused ion beam

For the FIB annular milling as final preparation process, a fs-laser rotation stage pre-prepared specimen with additional top-down laser circle ablation and 10 µm inner pattern diameter was chosen and processed with a FEI Versa 3D dual beam SEM/FIB workstation. Hereby, the parameters as depicted in Tab. 1 were used.

Tab. 1: FIB annular milling parameters of a fs-laser pre-prepared APT specimen.

step	outer diameter	step size	inner diameter	FIB voltage	FIB current	time per cut
1	35.0-15.0 µm	5.0 µm	6.5 µm	30 kV	7000 pA	15 - 20 s
2	10.0 - 3.5 µm	1.0 µm	3.0 - 1.5 µm	30 kV	3/1000 pA	10 - 15 s
3	3.0 - 2.0 µm	0.1 µm	1.4 - 0.5 µm	30 kV	500 pA	3 s
4	2.0 - 1.0 µm		0.5 - 0.2 µm	30 kV	100 pA	1 - 2 s
5	0.7 - 0.5 µm		0.2 - 0.1 µm	30 kV	30 pA	1 s
6	1.0 µm		0	5 kV	48 pA	variable
7	-			2 kV	27 pA	some s

3.5 (Post-)imaging

The initial specimen characterization during the preparation process was performed using light optical microscopes (LOM), preferentially the build-in cameras of the microPREP laser ablation system. With unclear imaging using the microPREP cameras or after the electropolishing process, either a Zeiss Axio Imager or a Zeiss Stereo Discovery.V20 were used to preselect specimens for further action. During the

micropolishing process, also photographs through the LOM were taken. Finally, SEM documentation was primarily conducted using a Tescan Clara with 10 kV electrons and an Everhart-Thornley or back-scattered detector (only if explicitly mentioned). The FEI Versa 3D dual beam SEM/FIB workstation was only used for imaging Fig. 21 with 20 kV and Figs. 49-51 with 10 kV electrons.

3.6 Atom probe tomography

All APT measurements were conducted using a CAMECA LEAP 5000 XR in voltage mode. The pulse fraction was set to 20 %, with a pulse frequency of 250 kHz and a detection rate of 0.5 % at a temperature of 50 K. The experiments were divided into the three preparation routes fs-laser & electropolishing, fs-laser & BIB milling and fs-laser & FIB annular milling. While for the specimens finished with BIB milling and FIB annular milling only one APT measurement was needed as proof of concept, for the electropolishing finish five attempts had to be made.

4 Results and discussion

4.1 fs-laser pre-preparation

4.1.1 x,y-stage: pre-cutting of blanks for atom probe tomography

Using the fs-laser to substitute low-speed precision saw or wire machining processes to cut out APT blanks enabled design freedom and operator time efficiency. Fig. 20 embodies both of them. Firstly, apart from the fabrication of ten standard rectangular blanks at the left-hand side, also ten slightly tapered blanks were cut out using the same CAD drawing. Secondly, before cutting the laser focus position (by simply adjusting the sheet into the microscope focus) and further parameters had to been set properly. The laser ablation itself did not require any external intervention during the process. Thus, the relatively long machine time requirement of approximately 15 h for 20 blanks could be moved into the night hours. One of the major advantages of the 1 mm thick sheet was that no additional Cu sleeve was needed during the whole APT specimen preparation and measurement process. Reducing the sheet thickness could have reduced the cutting time significantly, but without the advantage mentioned above. The resulting blanks themselves had a good shape, only a small taper of a few degrees in cutting direction, into the drawing plane of Fig. 20, could not be completely avoided using work angles of ± 5°. Since further laser ablation or thinning processes were conducted in the centre of the blank cross-section, where this taper was neglectable small, it did not affect the final shape of the APT specimen. The optimized shape described in section 3.1.2 showed a similar taper angle in work direction, but also no negative effects during further processing.

Fig. 20: Image of the result after cutting 20 APT blanks with a fs-laser ablation system out of a 1 mm thick Fe sheet, after cleaning with CO_2 snowjet.

4.1.2 x,y-stage: top-down ablation and thinning

This chapter gives priority to the effects of variations in laser focus shift, pattern size and geometry and the additional step for removal of secondary apexes on the resulting APT specimens. The length of almost constant diameter at the specimen apex was

mainly dependent on the focus shift parameters. Using the fs-laser with a constant focus position resulted in a faster increase in specimen diameter, whereas the apex diameter itself was smaller, resulting in a field emitter like shape (see image Fig. 21b). During processing, the current ablated area was moving further and further away from the actual focus spot. Furthermore, also the necessary reduction (factor 35-800) in cross-section of the specimen influenced the apex shape. For the first two examples of this section, standard rectangular blanks were used, whereas for the third one a slightly tapered blank was chosen. All examples described in this section were prepared using 2.5 W laser power for all individual steps. In Fig. 21a-d a top-down circle ablation specimen with an inner pattern diameter of 40 µm is depicted, processed in 16 min without focus shift and 251 repetitions. Hereby, the pattern (Fig. 21a) is shown as black lines and the specimen cross-section as bluish background. The secondary apexes, clearly visible in Fig. 21b and d, are the result of laser focus weakening during processing downwards the specimen. Concerning the APT measurement itself, the distance between specimen apex and secondary apexes is far from the required 50-100 µm minimum from section 2.1.2, but further process steps to finalize the specimen geometry could be affected. This will be discussed in particular in section 4.3. Furthermore, the specimen apex was slightly smaller than the actual laser pattern, visible in Fig. 21c, presumably due to the Gaussian distribution of the laser beam size.

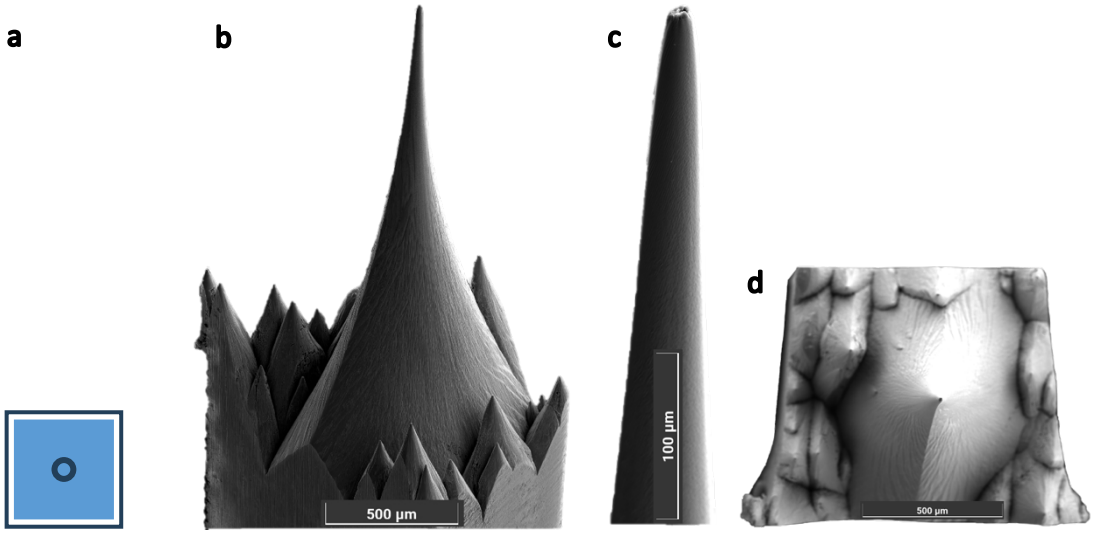

Fig. 21: Top-down fs-laser circle ablated APT specimen (40 µm inner pattern diameter and no focus shift), with (a) the pattern, (b) an overview SEM image, 45° tilted, (c) a detail SEM image of the apex, 45° tilted and (d) a top-view overview SEM image.

For comparison, the next example gives an overview of a slightly different approach. First of all, the circular inner pattern diameter was set to 20 µm, which represents a reasonable minimum for the adjusted 20 µm laser focus spot setting. Secondly, the focus shift was set to 500 µm at 100 focus levels and the number of repetitions was

increased to 501, which raised the preparation time to 25 min. Additionally, a step to remove secondary apexes was successfully implemented, with the focus fixed to the area of the apexes to be removed. After 126 repetitions and 7 min more preparation time the result is shown in an overview image in Fig. 22b, the transition of the apex to the rectangular remaining rod was almost evenly smoothened. Only some secondary apexes in the upper left and lower right corner of Fig. 22d remained after this process. The field emitter like shape was maintained, with a slightly longer area of almost constant diameter at the specimen apex and a slower increase in diameter, as particularly shown in Fig. 22c. Nevertheless, the area of constant diameter did not reach the full length of 500 µm (focus shift setting). Probably due to the huge amount of material that had to be ablated at once by reducing the cross-section by a factor of 800. Finally, Fig. 22e shows the detailed top-view with a smooth specimen apex and a resulting diameter of approx. 20 µm corresponding to the adjusted inner pattern size.

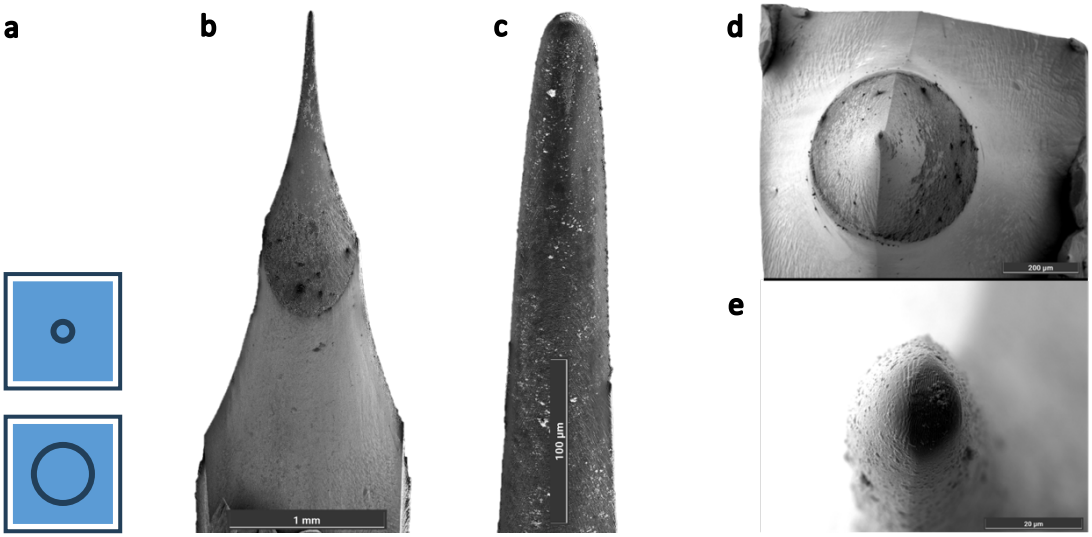

Fig. 22: Top-down fs-laser circle ablated specimen (20 µm final inner pattern diameter and laser focus shift), with (a) the patterns, and (b) an overview SEM image with almost entirely removed secondary apexes, (c) a detail, (d) and (e) top-view SEM images.

The last example for this section was prepared using the slightly tapered blanks and included an initial thinning step of the longer side of the 250x1000 µm^2 cross-section (see top pattern in Fig. 23a). Hereby, the specific laser parameters were 501 repetitions and 100 laser focus levels at 1000 µm shift for the 12 min lasting thinning process. This enabled a smaller cross-section of approx. 250x250 µm^2 for the subsequent circle ablation, with a 24 µm inner pattern diameter. Using a lower number of 350 repetitions compared to the previous example, but otherwise the same parameters, a much longer area of constant diameter was reached, as depicted in Fig. 23b and c. The detail top-view image in Fig. 23e shows a slightly elliptical specimen apex, but in the order of the inner pattern diameter of 24 µm. So, the implementation

of a focus shift made a big difference, if the reduction in cross-section between two steps was acceptably small (factor 35). Additionally, a final step to remove secondary apexes with 251 repetitions, 500 µm focus shift and 100 focus levels led within 12 min to the final shape with a smoothed surface at the bottom sides of Fig. 23b and d.

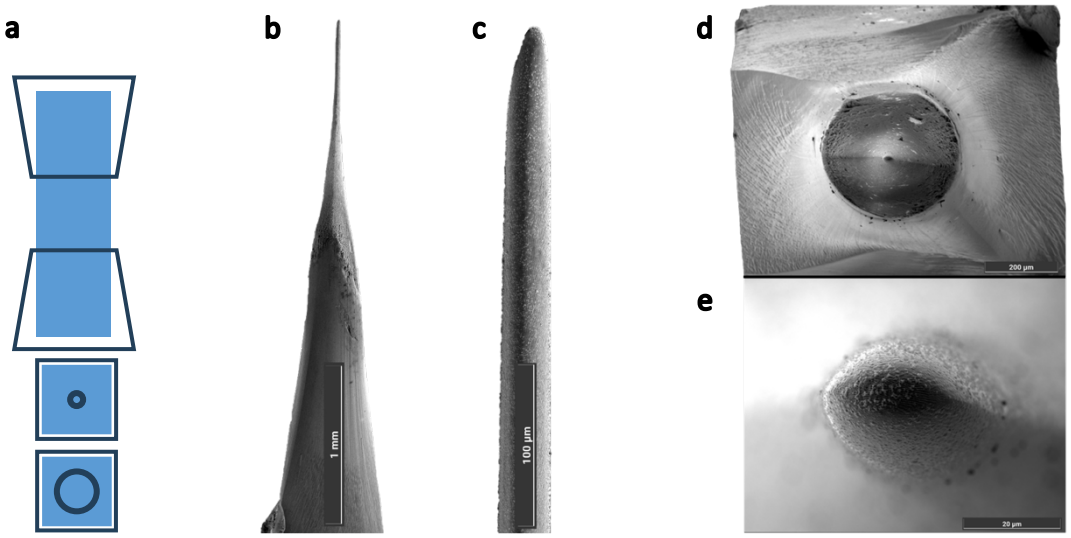

Fig. 23: fs-laser pre-prepared APT specimen, top-down pre-thinned and subsequent circle ablated (20 µm inner pattern diameter), with (a) the patterns, (b) an overview SEM image, (c) a detail of the specimen apex, (d) and (e) top-view SEM images.

4.1.3 x,y-stage: lateral thinning

Precursor material for the discussed examples in the following were the slightly tapered blanks, which slightly decreased the necessary preparation time for the first step. Furthermore, due to the different experimental setup of the lateral thinning process, the step to remove secondary apexes became unnecessary, and it was therefore omitted. Fig. 24b and d of the specimen discussed first support this decision, there is a smooth transition between the original width of 1000 µm and the two preparation widths of 100 and 40 µm without any extra apexes or protrusions. The final pattern is schematically shown in Fig. 24a. These values of the width were also reasonable lower limits concerning the mechanical stability of the specimen for the total preparation length of about 2 mm. Another point that appeared here for the first time was bending of the specimen apex as limiting factor for the final preparation length and width. Using 250 mW laser power, the limits were a maximum length of 500 µm and minimum width of 40 µm. Detail SEM images of the final shape with an almost square-shaped cross-section, are depicted in Fig. 24c and e.

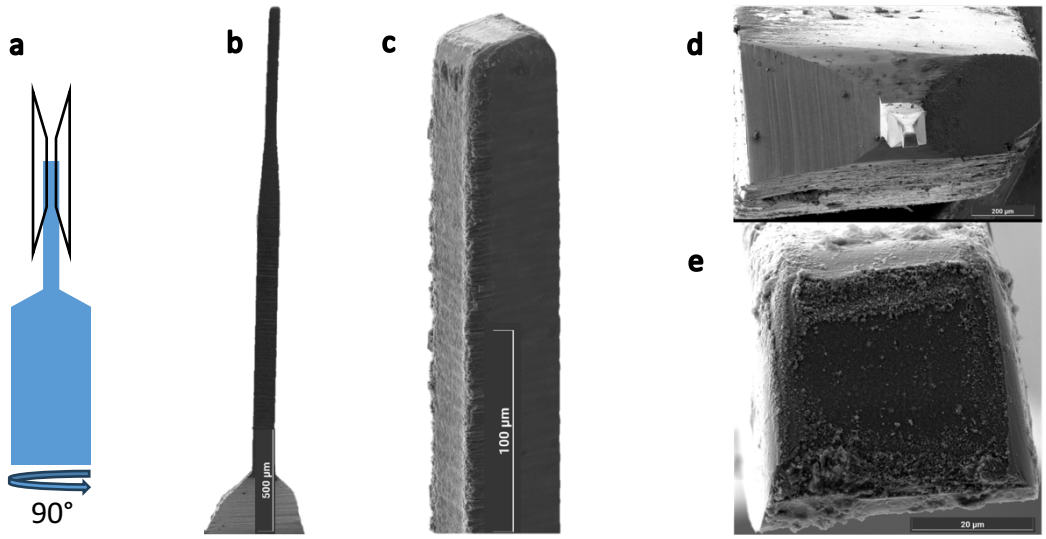

Fig. 24: fs-laser lateral thinned APT specimen, with (a) the pattern, (b) an overview SEM image, (c) a 40° tilted detail, (d) and (e) top-view SEM images.

Apart from finishing the fs-laser preparation at 40 µm, also experiments performing an additional step with 1 µm width of the end contour (Fig. 25a), to explore the limits of the fs-laser system, were conducted. Therefore, the laser power was further reduced from 250 to 100 mW. The small pattern distance of 1 µm led to a decrease in specimen length due to cutting of the specimen, ascribed to the laser beam size (8 µm FWHM) or imperfect alignment after the manual 90° rotation. This process led to an almost four-sided square pyramidal shape, as shown Fig. 25c and d.

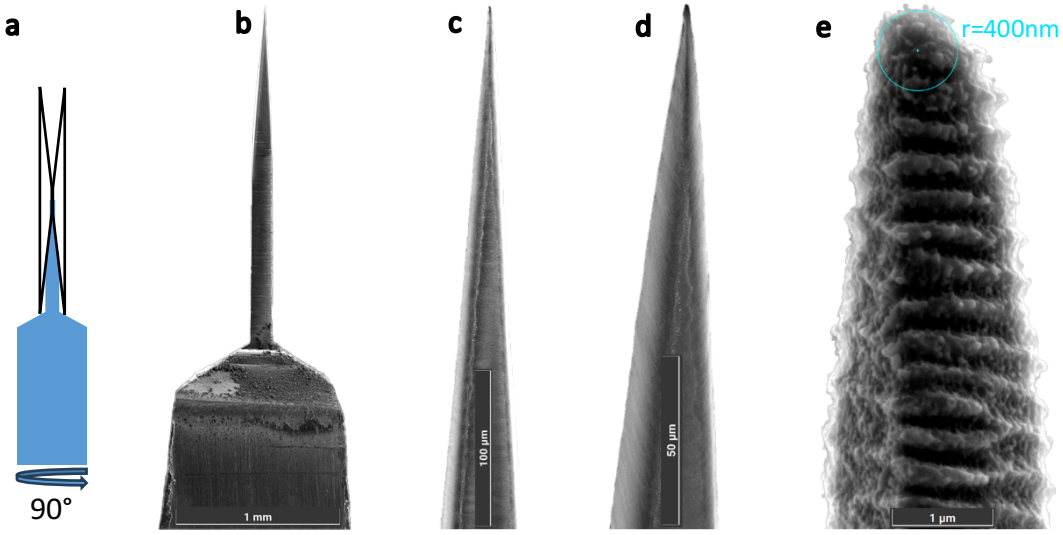

Fig. 25: fs-laser lateral thinned APT specimen with an additional sharpening step, schematically shown in (a), (b) and (c) SEM overview images, (d) a 40° tilted SEM image and (e) a SEM image of the specimen apex and a bluish circle (400 nm radius).

Similar as in the previous example, specimen bending also played a role here. In this context, the final preparation after the last manual 90° rotation was critical and the

success rate of reaching the desired shape was just about 50%. Some of the other specimens suffered from bending of the apex or became blade-shaped due to worse alignment of the pattern after the rotation. The SEM images depicted in Fig. 25b-e demonstrate a promising specimen, with increasing magnification from the left to the right-hand side. Fig. 25e shows a SEM image with a radius of the specimen apex of 400 nm, which is even below the adjusted width of the end contour. Furthermore, also laser-induced periodic surface structures were visible. Although having an apex radius almost in the order of magnitude for an APT measurement, the laser affected areas need to be removed with an additional sharpening and finishing process.

The results from the final experiments using custom shapes (individual laser patterns) in this section are shown in Fig. 26b-e. While using a shape without an area of constant diameter at the specimen apex led to a width of around 100 µm (Fig. 26b and c), the optimized shape (Fig. 26a) resulted in a desired specimen geometry of Fig. 26d. Even a slightly necked region below the specimen apex is visible in Fig. 26d and e, which can be useful for further micropolishing. Furthermore, the additional step to gently recut the original shape from the blank, proved to be useful to smoothen the surface.

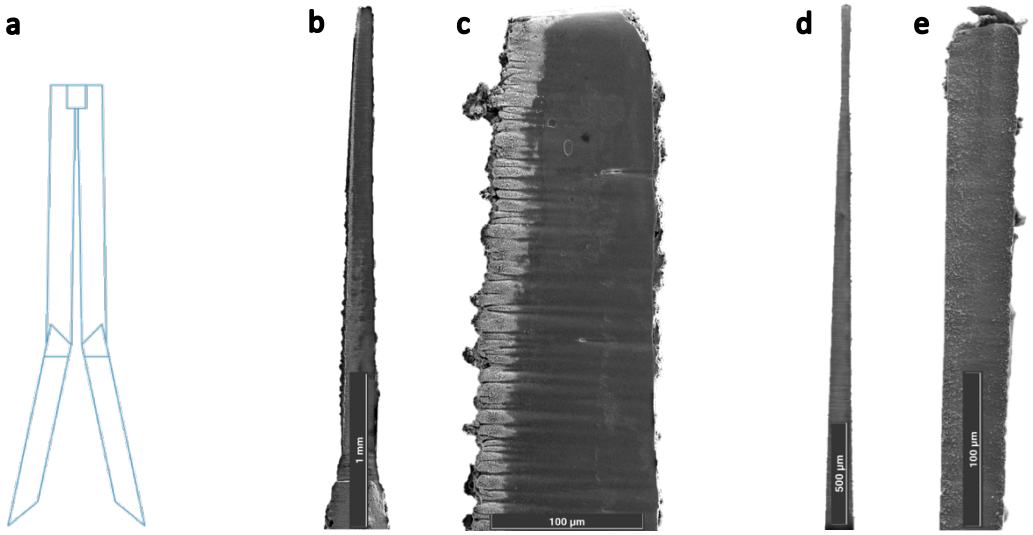

Fig. 26: Results of the fs-laser custom shape experiments, with (a) the pattern of the optimized shape, (b) and (c) SEM images of a regular custom shape specimen with 40 µm minimum width, (d) and (e) SEM images of the optimized shape with a longer area of constant width of 40 µm.

4.1.4 Rotation stage

In advance, cutting the 2 mm rods into a well-defined length of 12 ± 0.2 mm shall be discussed briefly. As already mentioned at the end of section 3.1.5, priority was given to preparation speed, which was achieved using the greatest possible focus shift while

cutting through the relatively thick rod (compared to the laser focus beam size in the µm regime). Movement of the z-axis, corresponding to the focus shift, was software-wise limited to 1350 µm, starting at a value of around 300 µm. Hereby, the negative effects on the centre of rotation proved to be neglectable, as the working area was big enough, especially compared to the low µm range of the APT specimen preparation examples shown in the following. The final cuts were smooth on the outside, slightly conical in the middle and the pieces reached the required length.

The first example of the actual APT specimen pre-preparation was the processing of a rectangular blank. Schematics of the essential laser patterns are depicted in Fig. 27a, including the additional process “removal of the edge”. Fig. 27b and d show the effects of this extra step on the bottom side and the resulting smooth transition from the apex to the blank, which can be beneficial in further processing of the specimen, at the cost of additional 15 min preparation time.

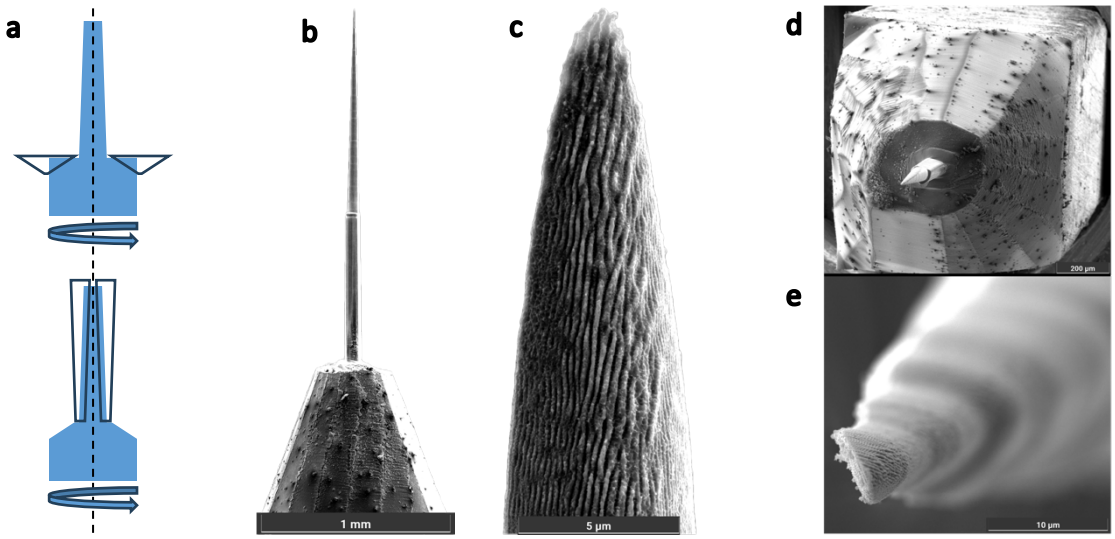

Fig. 27: fs-laser pre-prepared rectangular APT blank, using the rotation stage and 1 µm final distance between the patterns, with (a) schematics of the patterns (“removal of the edge” at the top), (b) and (c) side-view, (d) and (e) top-view SEM images.

There are two small jumps visible in Fig. 27b and d, which are due to the different pattern lengths of the individual steps. The final specimen apex after using 50 mW with 38 steps of 5° and 20 repetitions each is depicted in detail in Fig. 27c (side-view) and Fig. 27e (top-view). While the surface was smoothened performing several rotation steps, the apex itself became blade-shaped, and did not reach the desired conical shape. The most probable reason is, that the centre of rotation was not accurate enough to perform 38 steps with a 1 µm pattern distance at the exact same position. Therefore, the fs-laser beam must have hit the specimen also slightly below the apex and cut through the specimen. In the experiments and in the microPREP software the

arrangement was upside down, but the convention from Fig. 27 shall be used throughout this section, as all further figures are also depicted in this way. One more point concerning the rotation stage usage in general was the inconvenient specimen cleaning between preparation steps. CO_2 snowjet cleaning would have required the removal of the entire stage out of the fs-laser ablation system with the accompanying effects of necessary stage calibration and completely new rotation centre definition. For this reason and because of the small dimension of the final specimen apex, cleaning was performed gently using a compressed gas bottle at the end, resulting in a higher number of dust particles at the bottom side of the specimen.

In contrast to the example mentioned above, for the next one the 2 mm rod was used as precursor material. Nevertheless, the preparation process parameters were very similar, apart from two exceptions: On the one hand, the “removal of the edge” step was omitted, because no subsequent micropolishing was planned for this specimen type. On the other hand, the opening semi-angle of the specimen was increased from previous 2° to a higher angle of 5°, particularly visible in Fig. 28a.

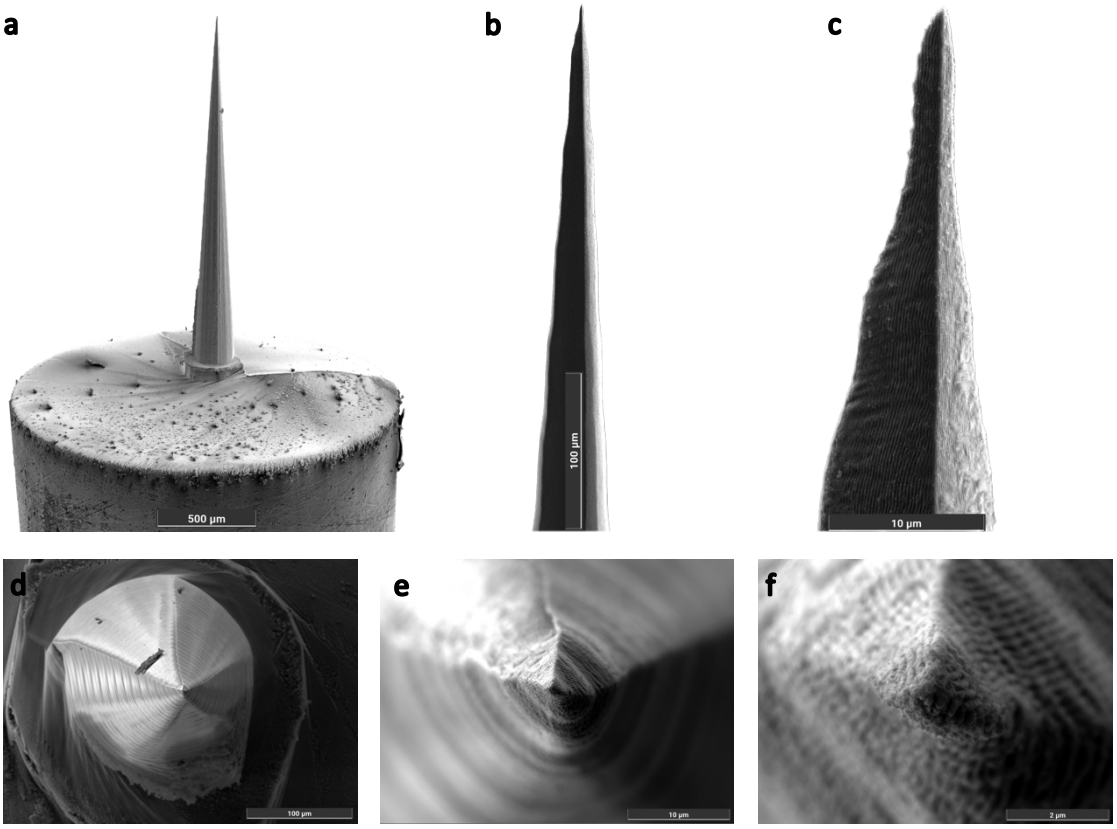

Fig. 28: APT specimen, pre-prepared using a 2 mm rod with the fs-laser rotation stage, three steps and a final distance between the patterns of 1 µm, with (a)-(c) side-view and (d)-(f) top-view SEM images.

The motivation for this was creating a shape closer to Fig. 2 from section 2.1.2, because the final preparation of this specimen should be performed with (ideally) equal

material removal using BIB milling. Another aspect of a higher semi-angle was increased robustness. Nevertheless, 38 steps of 5° with 1 µm pattern distance as final process turned out again as too close for an even finish towards the specimen apex, as shown by small jumps in Fig. 28b and c. Furthermore, especially visible in the top-view images Fig. 28d-f is a 6-sided pyramidal shape ending in a 4-sided pyramid at the apex, which was not in accordance with the adjusted rotation pattern step sizes. After the second process the shape should have been 18-sided and finally after the last process 36-sided. Again, the cause was probably a not exactly (re-)defined centre of rotation. Whereas the specimen apex itself was in the desired order of magnitude of 1 µm.

The next example is a comparison of the rotation stage with the results from x,y-stage lateral thinning (section 4.1.3). Hereby, after a preparation to a modest pattern distance of 30 µm, the last preparation step down to 1 µm distance was performed two-staged with a single semi-manual 90° rotation in between, as depicted in Fig 29a. For this preparation technique, a 4-sided pyramidal shape would have been the optimum, but the overview SEM image in Fig. 29b shows a blade-shape. Even though the 90° rotation was performed software-wise, and the centre of rotation was re-determined before this process, the positioning of the laser pattern after the rotation at the exact same position failed. Nevertheless, the specimen apex itself (Fig. 29c) was only moderately blade shaped, the region below was free from small jumps and the shank diameter increased smoothly.

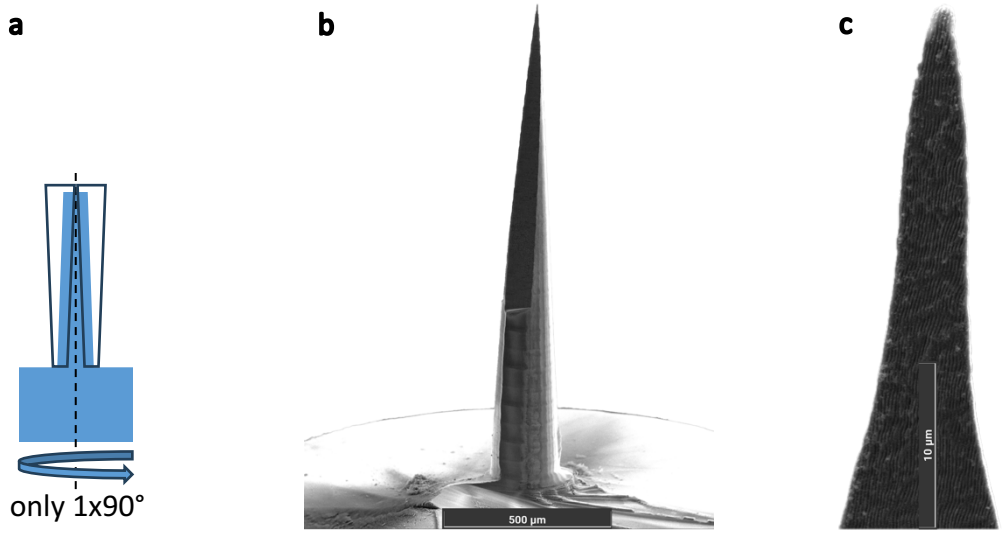

Figure 29: APT specimen, fs-laser pre-prepared from a 2 mm rod with the rotation stage, after a semi-manual 90° rotation step with 1 µm pattern distance as final process, with (a) the pattern, (b) a SEM overview image and (c) a SEM detail image.

As consequence of the sharp, but slightly blade-shape of the APT specimens after preparation with the rotation stage only, efforts were made to secure a circular

cross-section. The final step with 1 µm pattern distance from the previous examples was replaced by x,y-stage top-down ablation with a circular inner pattern, as described in section 3.1.5. So, for various specimens, the rotation stage preparation was primarily used as reduction of the cross-section diameter from 2 mm to 100-400 µm, which was achieved without any troubles. Subsequently, the top-down ablation experiments were conducted with an as low as possible inner pattern diameter. It turned out, that the lower limit was 8 µm, lower values resulted in unwanted material removal within the inner pattern, most probably based on the laser focus beam size (8 µm FWHM) in the same order of magnitude. In addition, the focus shift was limited to a maximum of 200 µm. Pushing both limits even led to the burst of a specimen with 4 µm inner pattern diameter. Both laser patterns, for the rotation stage and top-down circle ablation, are schematically depicted in Fig. 30a (top-down pattern enlarged). SEM images of a specimen, processed with a reasonable inner pattern diameter of 10 µm are shown in Fig. 30b and c. The reduced laser power, compared to the top-down ablation only experiments, of 100 mW led to a smooth surface of Fig. 30c without any jumps in diameter. Furthermore, the small secondary apexes of Fig. 30b did not affect further processing of the specimen.

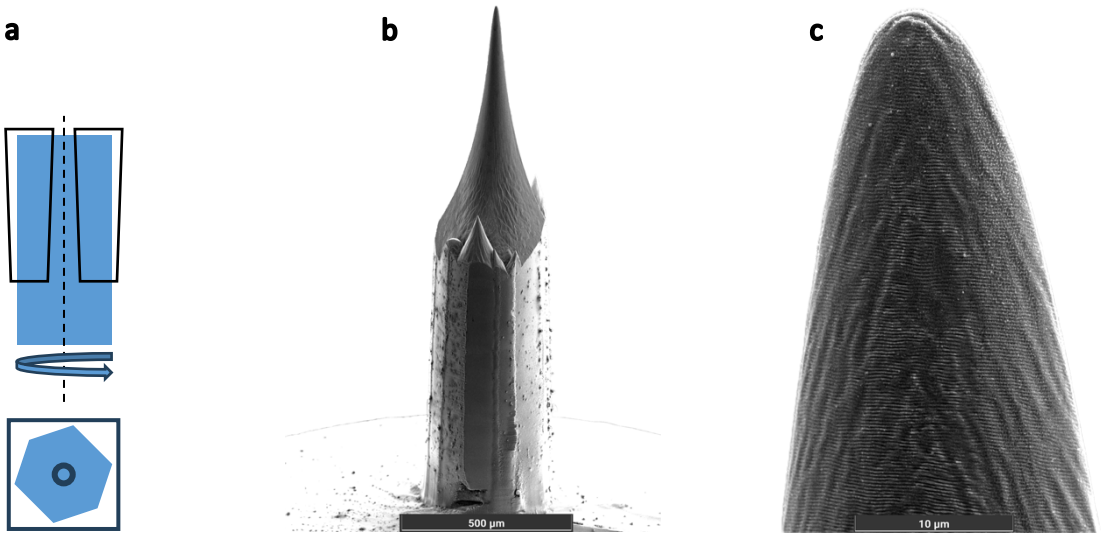

Fig. 30: APT specimen, pre-prepared from a 2 mm rod, using the rotation stage and subsequent top-down circle ablation with 10 µm inner pattern diameter, with (a) schematics of the patterns for the rotation stage and the final top-down circle ablation, (b) an overview SEM image and (c) a SEM image of the specimen apex.

4.2 Electropolishing

For this rather small series of experiments the rectangular blanks with 1x1 mm^2 cross-section, previously shown on the left-hand side of Fig. 20 in section 4.1.1, were used, without further fs-laser processing. Hereby, the fs-laser should just replace the conventional low-speed precision saw or wire machining step without any special sharpening of the blanks. These blanks were the only ones in this work, that were additionally prepared with electropolishing step 1. Due to the greater cross-section of the blanks than the commonly used dimensions of 300x300 μm^2 up to 500x500 μm^2 [4,6], the preparation time of 25-30 min for step 1 was relatively high. The necessary change of the electrolyte 1 and even of the inert layer because of heat development, consumption and pollution of the liquids contributed significantly to this. Final step 2 micropolishing of these specimens was, due to a higher starting diameter after step 1, more demanding compared to all further fs-laser processed specimens. This, together with less operator skills at the time of preparation, led to high radii of the specimen apex of 200 nm and above.

4.3 fs-laser & electropolishing

In the course of the experiments the idea to prepare blanks for step 1 electropolishing was quickly discarded. All following specimens were processed to a sufficiently low cross-section for direct step 2 micropolishing. Otherwise, the advantage of implementing the fs-laser ablation process into the APT specimen preparation would not have justified the extra effort. To reach these requirements, the upper limit for the specimen apex was a diameter/edge length of around 40 µm. Hereby, there was no significant difference between a circular or quadratic shape. Nevertheless, also specimens with slightly bigger dimensions were successfully micropolished.

4.3.1 x,y-stage: top-down ablation

At first the influence on micropolishing of secondary apexes resulting from laser ablation shall be discussed and if the removal was worth the extra preparation time. This topic was not relevant elsewhere using a lateral thinning configuration or the rotation stage, where the preparation direction was perpendicular to the specimen. Fig. 31a-c shows photographs taken through the LOM while micropolishing a top-down ablation specimen with an inner pattern diameter of 60 µm with remaining secondary apexes. The typical field-emitter like apex with a rapid increase in diameter is depicted in Fig. 31a directly before micropolishing. Preparation of the specimen by dipping into

the Au loop filled with electrolyte 2 (Fig. 31b) worked perfectly until the situation in Fig. 31c was reached: while trying to move the specimen on the right-hand side of the loop around a distinct position back and forward to form a necked region, the electrolyte droplet was sucked in from the secondary apexes. Apparently, there were many small channels that cause capillary forces. Further micropolishing was only possible, if the electrolyte droplet was exchanged and reached the right size by chance. The final preparation on the left-hand side of the loop was not affected at all. Therefore, the removal of secondary apexes did not only offer more appealing SEM images, but also contributed to the preparation success for the micropolishing step.

Fig. 31: Photographs through the LOM in the etching lab during step 2 micropolishing of a top-down circle ablation specimen with 60 µm inner pattern diameter without removal of secondary apexes, with (a) directly before step 2, (b) and (c) during step 2 after 2 min of preparation time, demonstrating capillary forces between the electrolyte and the secondary apexes.

For the experimental series of top-down circle ablation, preferentially specimens with removed secondary apexes or with previously conducted thinning (top-down or lateral) were chosen, so that the effects mentioned above were neglectable small. Starting with a diameter of 40 µm at the specimen apex, resulted in some minutes of necessary pre-thinning with an increased voltage of 10 or 12 V before starting the actual necking process at the right-hand side of the loop. Due to the small volume, the electrolyte 2 was quickly exhausted and had to be replaced at least once per specimen. Also, for specimens with 30 µm apex diameter some pre-thinning was helpful, but not mandatory, reducing the preparation time from 7-10 min to around 5 min. Only when the diameter was decreased to 20-24 µm a fast and reproduceable immediate neck on the right-hand side of the loop could be formed within 3-5 min, with a fast voltage decrease from 10 to 8 V. Images of a specimen pre-prepared with top-down thinning and final top-down circle ablation with 24 µm inner pattern diameter (section 4.1.2: Fig. 21) are depicted in Fig. 32a-c. The resulting apex radius after micropolishing for 3 min using 8 V only was 70 nm (Fig. 32c). Unfortunately, there was a two-week delay in SEM imaging, resulting in corrosion artefacts and only one acceptable specimen.

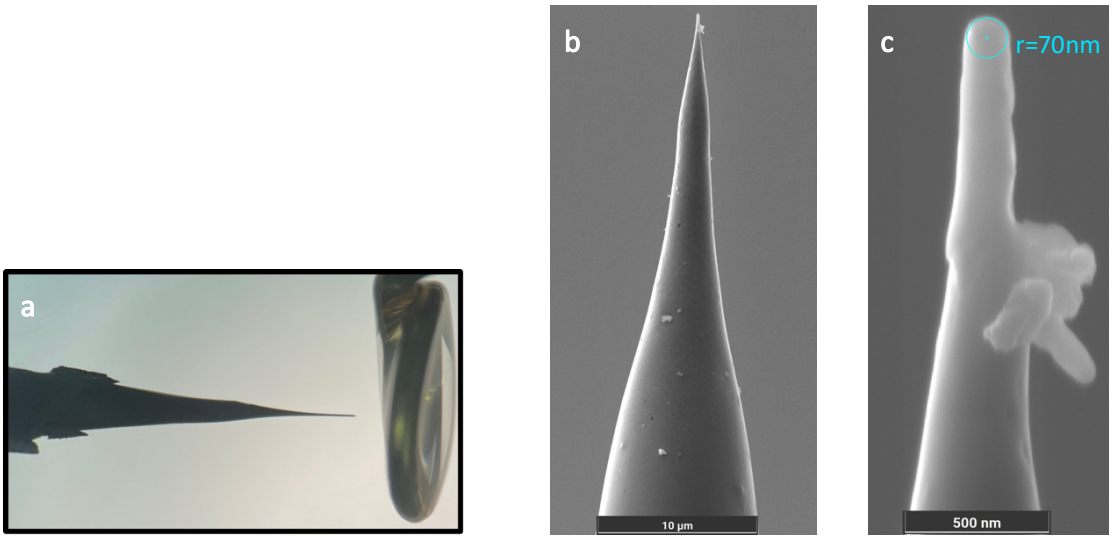

Fig. 32: A fs-laser pre-prepared APT specimen, top-down pre-thinned and circle ablated (section 4.1.2: Fig. 23), with (a) a photograph through the LOM in the etching lab directly before micropolishing, (b) an overview image SEM image after micropolishing and (c) a detail SEM image with a bluish circle (70 nm radius) and some corrosion artefacts below due to two weeks of unplanned storage.

4.3.2 x,y-stage: lateral thinning

Although the specimen from Fig. 32 showed some preparation comfort during micropolishing due to the long thin apex shape and the gentle transition to the rectangular base, they were surpassed in this by the lateral thinning specimens. The only negative effect of this long area with a small diameter was the decreased mechanical stability, which occurred later on during the proof of concept APT measurements. Hereby, the specimen movement with the tweezers and the positioning on the APT puck provided some difficulty, especially for a specimen pre-prepared with custom shapes.

The first discussed lateral thinning specimen was processed to 20 µm width of end contour with 250 mW and hence showed a slight bending of the specimen after the fs-laser process ("standard lateral thinning" in Fig. 33a). For this reason, the necking was performed further away from the apex and after a first unsatisfying micropolishing, a second necked region was prepared. The result with an apex radius of 60 nm after 8 min preparation time using 10 and 8 V is shown in SEM images in Fig. 33c-e. Other specimens performed equally well, even if the preparation time compared to the previous section 4.3.1 was slightly increased due to larger starting diameters of 20-50 µm.

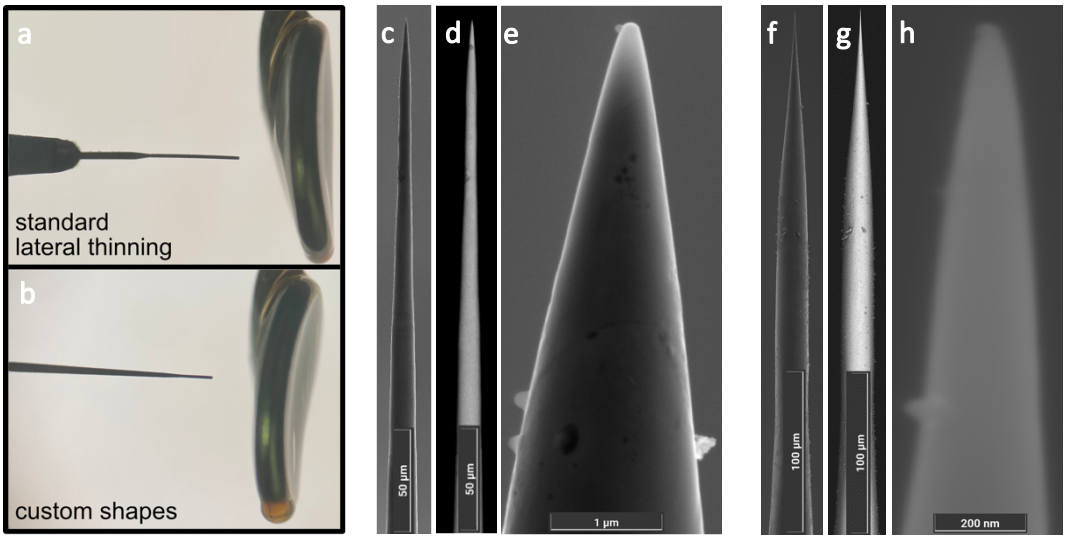

Fig. 33: fs-laser pre-prepared APT specimens, (a) and (b) showing photographs through the LOM in the etching lab directly before micropolishing, and (c)-(h) SEM images after micropolishing of (c)-(e) a standard lateral thinning specimen resulting in 60 nm apex radius, and (f)-(h) a lateral thinning specimen using custom shapes resulting in 25 nm apex radius. A back-scattered electron detector was used for imaging the overview SEM images in (d) and (g).

Concerning the custom shape experiments, the end diameter of 100 µm (section 4.1.3: Fig. 26a and b) was clearly too thick for the regular micropolishing process. Additional 10-12 min of pre-thinning with 12-13 V did not prove any advantage of using the fs-laser as pre-preparation step. Out of three prepared specimens, one got damaged due to overheating in the electrolyte 2 droplet, one was discarded after LOM imaging and the only SEM imaged specimen had an apex radius of 160 nm and is not depicted here. Whereas the fs-laser pre-prepared custom shape specimens with the longer area of constant 40 µm edge length (section 4.1.3: Fig. 26c and d) performed well and reproduceable. Photographs taken through the LOM in the etching lab directly before micropolishing are depicted in Figs. 33b and 34a. The final micropolishing process resulted in very similar apex radii of 25 and 24 nm, as shown in the SEM images Fig. 33f-h and Fig. 34c and d. Both specimens were prepared within 8 min using 10 and 8 V. If desired, a custom shape with 20-30 µm end contour within a slightly longer area of constant edge length and reduced laser power during the preparation process could be used to optimize the shape for time efficient micropolishing.

The next specimen was fs-laser prepared with this aspect in mind and was not explicitly discussed in section 4.1. After the standard lateral thinning process without using custom shapes, subsequent top-down circle ablation with 20 µm inner pattern diameter was applied. This led to a similar shape compared to the top-down only processed specimens from Fig. 23, but without the necessity of removal of secondary

apexes. This process was very useful for successful and fast micropolishing. Fig. 34e-g shows such a specimen with an apex radius of 74 nm after micropolishing 3 min using 8 V. Furthermore, additional top-down circle ablation could also be applied on the less successful custom shape of Fig. 26a and b, mentioned above, with an end contour of 100x100 µm^2, in order to guarantee a small diameter of around 20 µm, in absence of specimen bending or resulting secondary apexes.

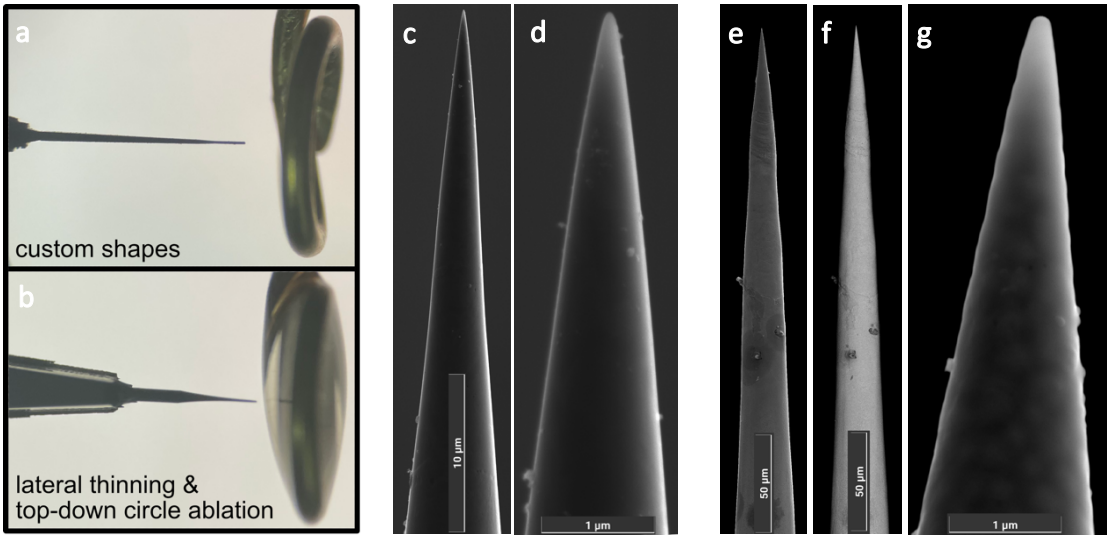

Fig. 34: fs-laser pre-prepared APT specimens, with (a) and (b) photographs through the LOM in the etching lab directly before micropolishing, and (c)-(g) SEM images after micropolishing of (c)-(d) a lateral thinning specimen using custom shapes resulting in 24 nm apex radius, and (e)-(g) a lateral thinning and subsequent top-down circle ablation specimen resulting in 74 nm apex radius. A back-scattered electron detector was used for imaging the overview SEM image in (f).

4.3.3 Rotation stage

The rotation stage combined the advantages of top-down ablation (small end diameters) and lateral thinning (long thin area without secondary apexes or bigger steps near the preparation area), mainly at the cost of increased preparation time. Considering the aspects of micropolishing after fs-laser pre-preparation mentioned in the last two sections, the rotation stage specimens looked promising for this task. Indeed, micropolishing these specimens down to small apex radii turned out to be fast and reproduceable. Due to the small specimen diameters and the low shank angle of 4-10° after fs-laser ablation, the preparation process resulted in very similar parameters of 1-3 min micropolishing using 8 V. In some cases, when the dimensions after fs-laser ablation reached the low µm regime, the necked region during micropolishing could hardly be differentiated from the remaining part of the specimen.

So, a further reduction in diameter would not be recommended. Two specimens are depicted in Fig. 35, with etching lab images before micropolishing (Fig. 35a and b) and SEM images after micropolishing (Fig. 35c-h). The fastest micropolished specimen within this work, prepared in 1 min, is shown in Fig. 35c and d and had an apex radius of 24 nm. Whereas Fig. 35e-h show a specimen, which was prepared twice, initially (Fig. 35e and f) and after one month of storage (Fig. 35g and h) the identical apex radius of 20 nm was reached. In the course of micropolishing these two specimens, the additional "removal of the edge" did not lead to differences in the preparation outcome. Nevertheless, for differently sized electrolyte droplets or especially for shorter fs-laser pre-preparation lengths the "removal of the edge" step would be useful to avoid possible electrical shortcuts between specimen and Au loop.

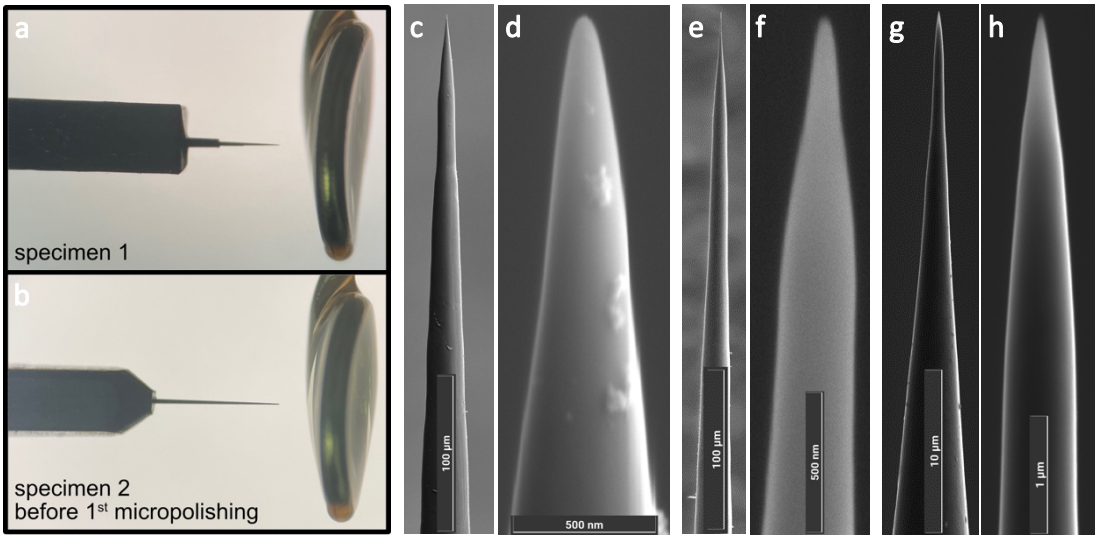

Fig. 35: fs-laser pre-prepared APT specimens, using the rotation stage, with (a) and (b) photographs through the LOM in the etching lab directly before micropolishing, and (c)-(h) SEM images after micropolishing, with (c) and (d) specimen 1 with resulting 24 nm apex radius, (e) and (f) a different specimen 2 with 20 nm apex radius, (g) and (h) the previous specimen 2 newly polished with 20 nm apex radius as well.

4.3.4 Proof of concept APT measurement

In advance, it should be mentioned, that the fs-laser & electropolishing specimens were susceptible to fracture events. The APT measurement of the first specimen (rotation stage only) started early, below 2 kV, but fractured during the transition from manual to automatic voltage control at around $5x10^5$ ions. Proceeding with two newly polished rotation stage specimens, one of them previously shown in Fig. 35e and f, also led to early fracture. Finally, a lateral thinned custom shape specimen (Fig. 34c and d), was successful measured in the APT reaching 9.7 million detected counts. The

associated voltage curve is depicted in Fig. 36a and the 3D reconstruction of all atoms in Fig. 36b.

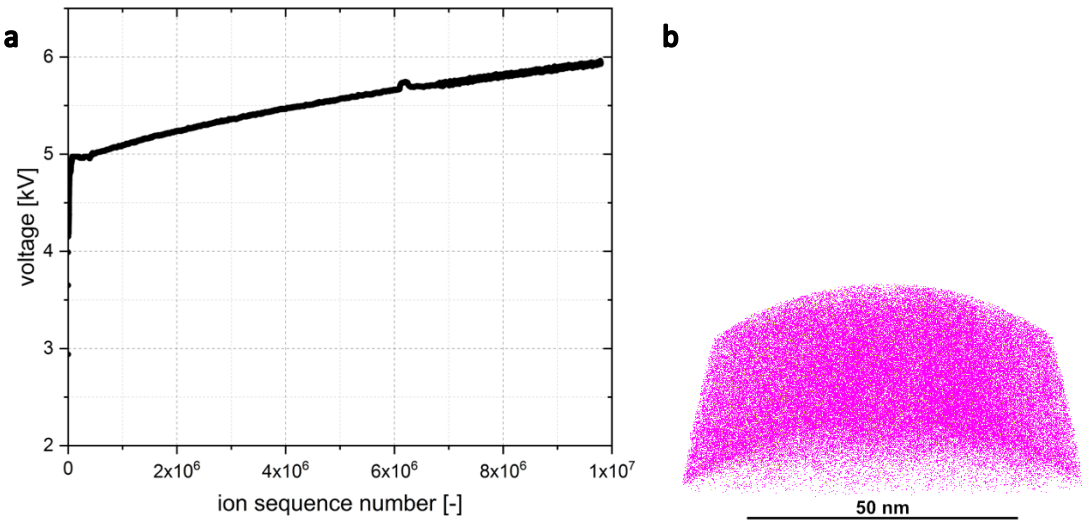

Fig. 36: Proof of concept APT measurement of the process route fs-laser & electropolishing, with (a) the voltage curve and (b) the 3D reconstruction of all atoms.

Due to the high background level of 200 ppm/ns, the peaks were difficult to distinguish from the background. Therefore, only Fe as main element, with Cr and Mn as accompanying elements were detectable, limiting the comparability between the APT measurements of the specimens finished with BIB milling or FIB. Fig. 37 shows the corresponding mass spectra curve with embedded bulk decomposition.

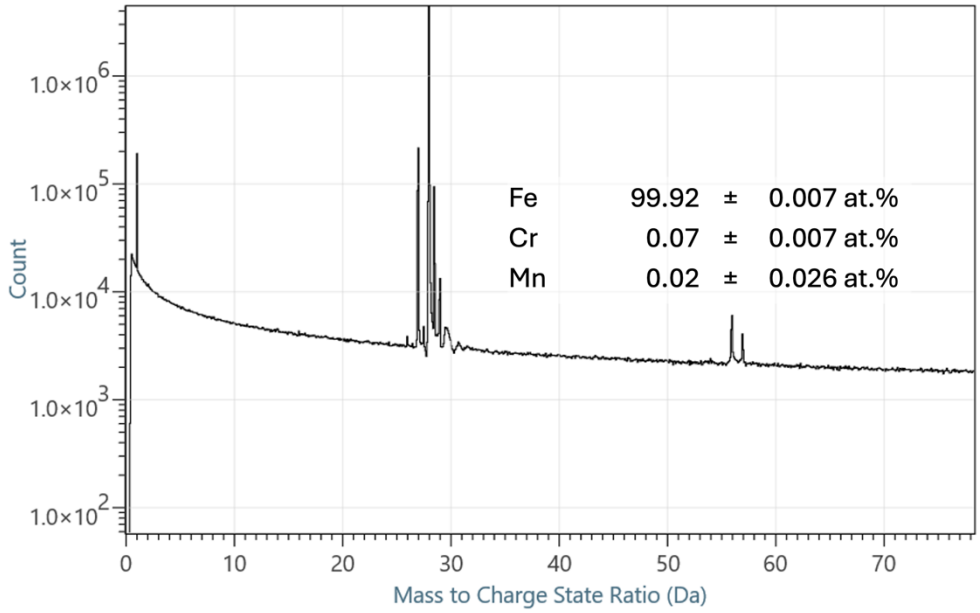

Fig. 37: Mass spectra (black line) with embedded bulk decomposition details of the proof of concept APT measurement of the process route fs-laser & electropolishing.

4.4 fs-laser & broad ion beam milling

For the BIB milling experiments discussed in the following the rods with 2 mm diameter were used exclusively, always initially fs-laser prepared with the rotation stage, with an optional additional top-down circle ablation step. Hereby, fitting into the Al adapter (section 3.3: Fig. 19) with pliers worked well, independent from the final fs-laser process parameters, due to the same dimension on the bottom of the specimen and a similar preparation length. Slight variations in the specimen length were of greater importance concerning the incoming broad Ar^+ ion beam. If necessary, a manual adjustment of the Al adapter position was conducted. Furthermore, the tilt angle β was kept constant at 35° in the following sections 4.4.1 and 4.4.2.

4.4.1 Rotation stage

First of all, due to the lack of experience using this preparation technique for finishing fs-laser pre-prepared APT specimens, the required time needed to achieve a visible effect using low energy Ar^+ ions was investigated. For this purpose, a rotation stage only prepared specimen with 1 µm final pattern distance and 5° opening semi-angle of the pattern was chosen (section 4.1.4: Fig. 28). BIB milling was performed using an acceleration voltage (V_{acc}) of 2 kV and 5 min steps, inspired by the work of Herbig et al. [14]. The results from the SEM investigations are shown in Fig. 38a-c and only show a slightly smoothened surface, but no reduction in size within 15 min preparation time. Starting without oscillation (osc.), the last 5 min were performed using a 0.5 turn osc.

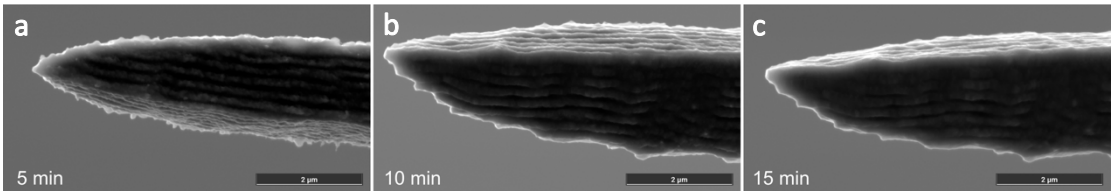

Fig. 38: First BIB milling experiments of a fs-laser pre-prepared APT specimen (section 4.1.4: Fig. 28), using V_{acc} = 2 kV and β = 35° in 5 min steps from (a) to (c).

Therefore, longer preparation times were chosen, with the results after additional 60 min using V_{acc} = 2 kV and 0.5 turn osc. depicted in Fig. 39a-f, using three different SEM stage tilt angles. Starting on the left-hand side with the same view as in Fig. 38, a clear reduction in dimension and a sharpening of the specimen apex with a modest shank angle is visible in Fig. 39a and d. For a more precise examination of the shape after BIB milling the SEM stage was tilted, resulting in a visible blade-shaped specimen (Fig. 39b and e), mirroring the blade shape from the fs-laser rotation stage preparation. Further stage movement (Fig. 39c and f) confirmed this, indicating even

material removal at the specimen apex with the resulting shape strongly dependent on the original shape after the fs-laser pre-preparation.

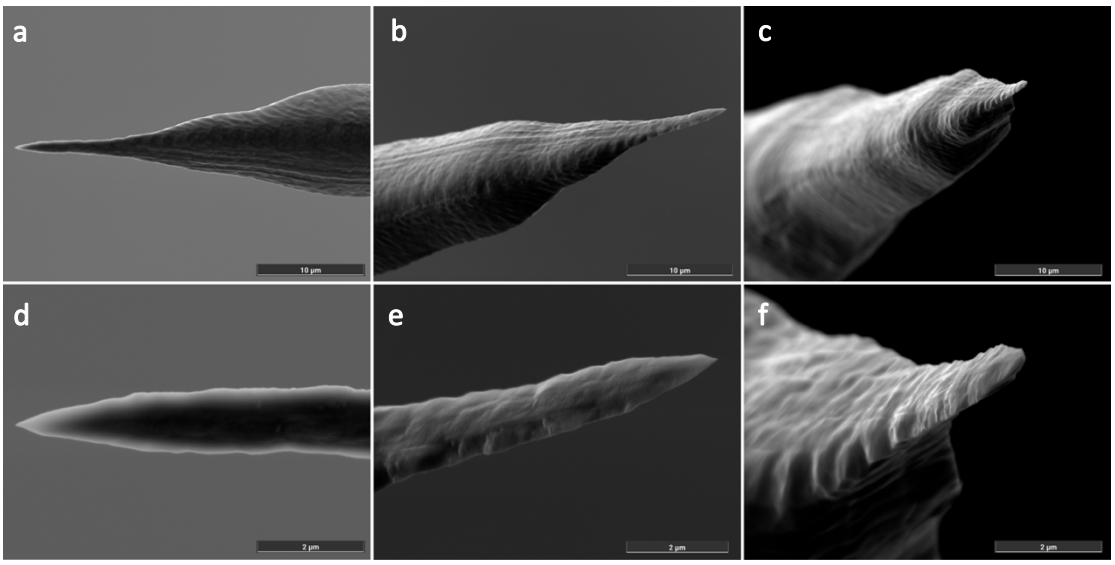

Fig. 39: SEM images using three different SEM stage tilt angles of a fs-laser rotation stage pre-prepared APT specimen (section 4.1.4: Fig. 28), finished with BIB milling using V_{acc} = 2 kV, β = 35°, 0.5 turn osc. within 75 min: (a), (b) and (c) showing overview images, (d), (e) and (f) the corresponding detail images.

Finally, an even more vivid example of this problem is depicted in Fig. 40a-f. Starting with a distinct blade shape (Fig. 40a and b) after the fs-laser, followed by BIB milling with V_{acc} = 2 kV, 0.5 turn osc. for 60 min (Fig. 40c), analogous to the previous specimen, did not result in sufficient sharpening of the specimen apex.

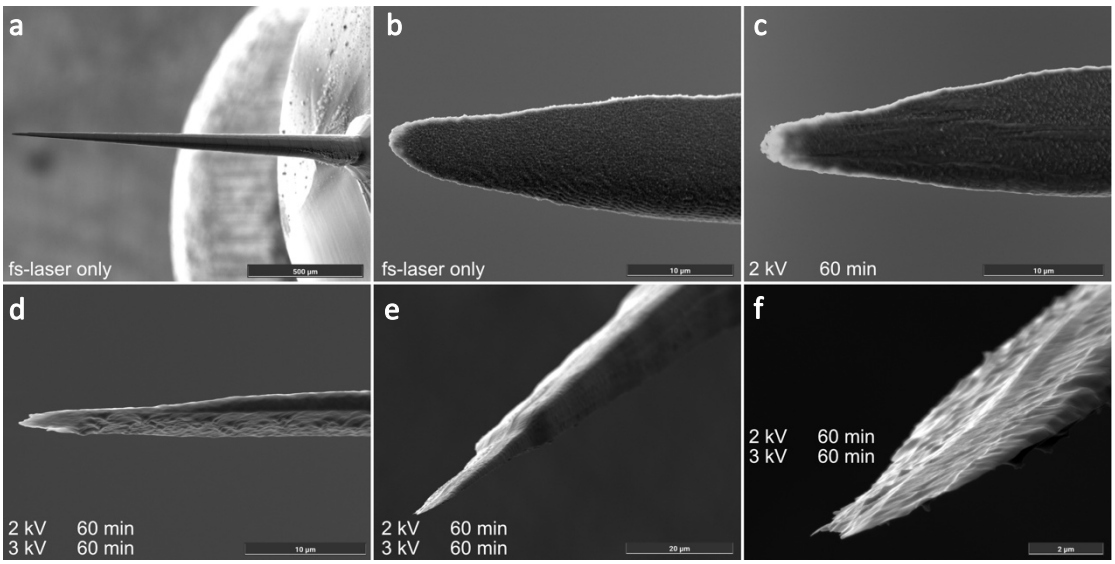

Fig. 40: (a) and (b) fs-laser pre-prepared APT specimen using the rotation stage, (c) after BIB milling using V_{acc} = 2 kV, β = 35°, 0.5 turn osc. for 60 min and (d)-(f) after additional BIB milling using V_{acc} = 3 kV, β = 35°, 0.5 turn osc. for 60 min.

Additional 60 min of BIB milling with increased V_{acc} to 3 kV, while remaining the 0.5 turn osc., massively reduced the specimen apex size, but led to a pronounced blade shape, without a clearly visible primary apex (Fig. 40d-f).

4.4.2 Rotation stage & top-down circle ablation

In order to overcome the problem with blade-shaped specimens after BIB milling, mirroring the original shape from the fs-laser, the additional top-down circle ablated specimens were chosen for this section. At the cost of a higher radius at the specimen apex, those specimens were almost circle-shaped. Two such specimens with different outcomes will be discussed in the following. At first, a specimen with final top-down ablation inner pattern diameter of 10 µm (section 4.1.4: Fig. 30) was processed with BIB milling for 120 min using V_{acc} = 3 kV without osc. and is depicted in Fig. 41a. Because of the insufficient reduction in apex size, two another attempts without osc. were performed, one using V_{acc} = 2 kV for 90 min (Fig. 41b) and another one using additional 3 kV for 120 min (Fig. 41c). Despite visible reduction in size, omitting the oscillation might have reduced the period in which the specimen apex was hit by the 3 kV Ar^+ ion beam. Therefore, a last attempt with 0.5 turn osc., but increased V_{acc} of 4 kV was performed. The result (Fig. 41d) was sharpening of the specimen, but also appearance of a double apex.

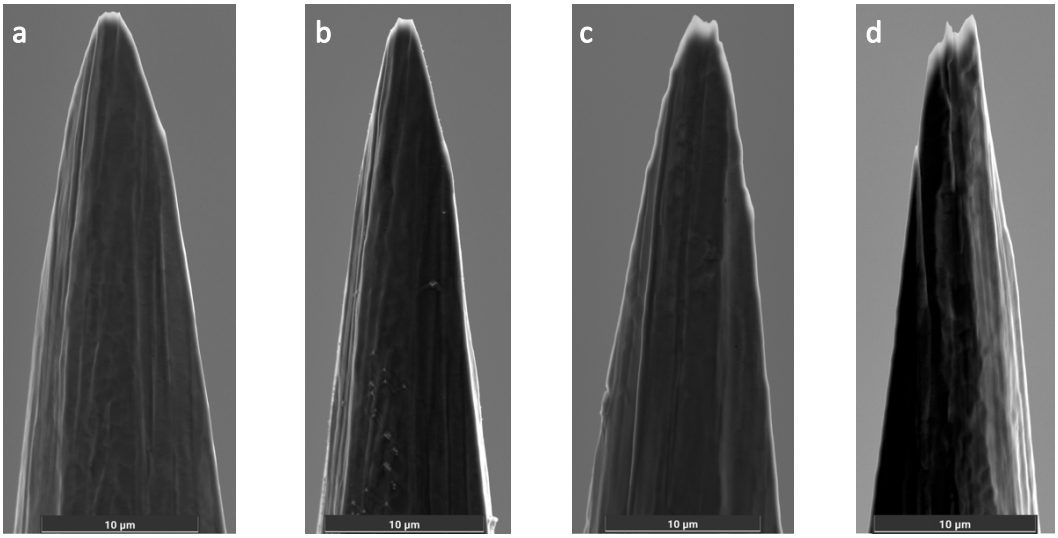

Fig. 41: SEM images of a fs-laser pre-prepared APT specimen using the rotation stage and top-down circle ablation (10 µm inner pattern diameter, section 4.1.4: Fig. 30), after finishing with BIB milling using β = 35° at four different stages: (a) V_{acc} = 3 kV for 120 min, (b) additional 90 min with V_{acc} = 2 kV, (c) another 120 min using V_{acc} = 3 kV, all without osc. and (d) final 60 min using V_{acc} = 4 kV with 0.5 turn osc.

The other specimens with final top-down ablation inner pattern diameter of 20 µm had a completely different outcome, despite similar starting conditions (shape in Fig. 42a) and BIB milling parameters. After 90 min using 3 kV and 0.5 turn osc., the apex blunted (Fig. 43b) and further processing was discarded.

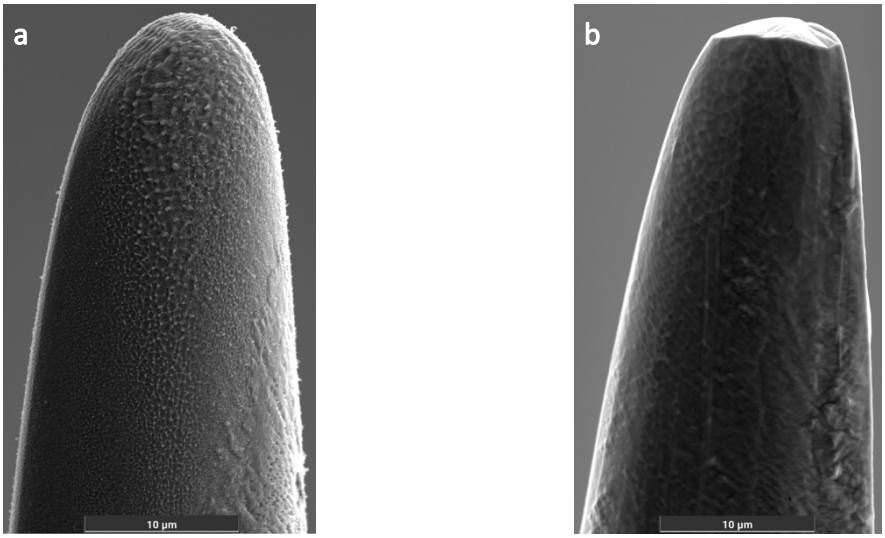

Fig. 42: SEM images of an APT specimen, (a) fs-laser pre-prepared using the rotation stage and top-down circle ablation (20 µm inner pattern diameter) and (b) after finishing with BIB milling 90 min using V_{acc} = 3 kV, β = 35° and 0.5 turn osc.

4.4.3 Tilt angle variations

After having conducted experiments with different initial shapes and slightly varying the process parameters V_{acc} and time, the last constant value to date, the tilt angle β, was changed for the last BIB milling experiments. The first discussed specimen started once again slightly blade-shaped after the fs-laser pre-preparation with the rotation stage and final top-down circle ablation with 8 µm inner pattern diameter, as depicted in Fig. 43a. Subsequent BIB milling with β = 35°, V_{acc} = 3 kV without osc. for 90 min did not change the shape significantly (Fig. 43b). Only when β was changed to 60°, BIB milling with V_{acc} = 3 kV and 0.5 turn osc. for 120 min led to a sharpening effect (Fig. 43c). But apart from sharpening the specimen apex, also some secondary apexes and other protrusions were generated in a distance below 10 µm. This detection is consistent with another specimen, which was fs-laser pre-prepared with the rotation stage only and 1 µm final pattern distance (section 4.1.4: Fig. 27). Subsequent BIB milling parameters were identical to those of Fig. 43c: β = 60°, V_{acc} = 3 kV and 0.5 turn osc. for 120 min. The resulting SEM image in Fig. 44 shows multiple apexes and even got useless for further processing due to bending of the very sharp primary apex during BIB milling at β = 60°.

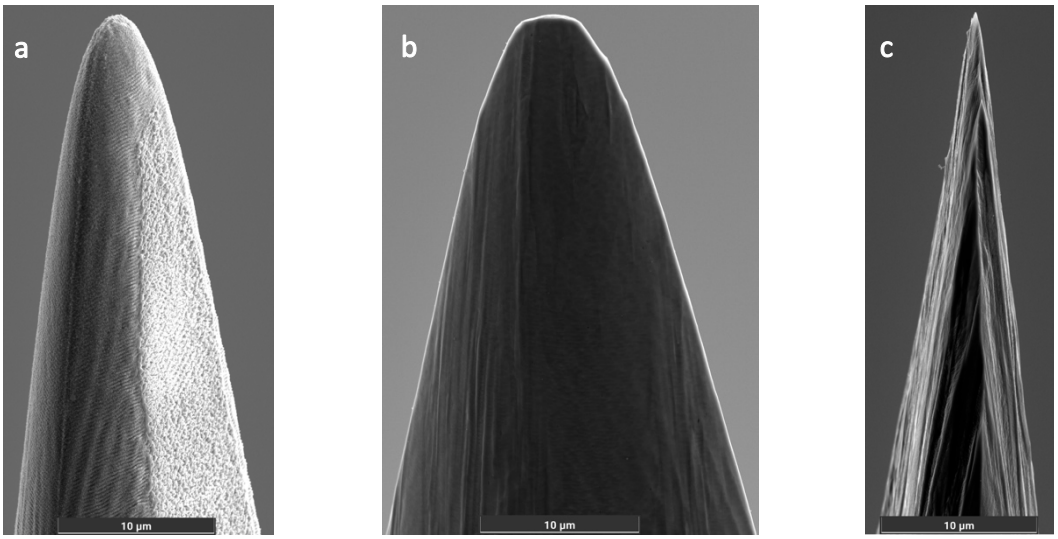

Fig. 43: SEM images of an APT specimen after (a) the fs-laser pre-preparation using the rotation stage and top-down circle ablation (8 µm inner pattern diameter), (b) subsequent BIB milling using β *= 35°and* V_{acc} *= 3 kV for 90 min and (c) final BIB milling with a different tilt angle* β *of 60°,* V_{acc} *= 3 kV, 0.5 turn osc. for 120 min.*

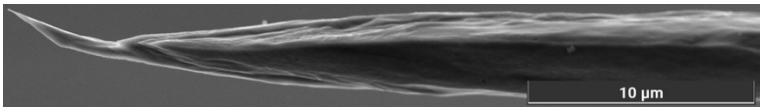

Fig. 44: SEM image, demonstrating the bending of the primary apex of an APT specimen, after fs-laser rotation stage only pre-preparation (1 µm pattern distance, section 4.1.4: Fig. 27) and finishing with BIB milling using β *= 60°,* V_{acc} *= 3 kV, 0.5 turn osc. for 120 min.*

Finally, after mixed results (blunting or sharpening) with β = 35° and unreasonable strong sharpening at β = 60°, experiments with β = 15° were conducted. Hereby, the fs-laser rotation stage specimen with the pyramidal shape caused by a single 90° rotation during the preparation process (section 4.1.4: Fig. 29) was used. Further BIB milling with β = 15°, V_{acc} = 3 kV, and 0.5 turn osc. for 120 min led to the promising results of Fig. 45. No signs of secondary apexes were detected in the overview SEM image (Fig. 45a) and the sharpening of the specimen led to a radius of 32 nm at the specimen apex, with a modest shank angle, as shown in the detail SEM image in Fig. 45b.

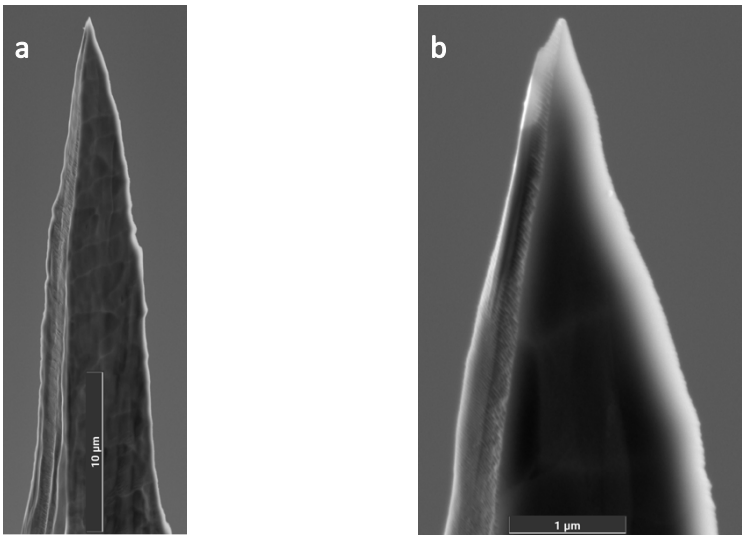

Fig. 45: fs-laser pre-prepared APT specimen using the rotation stage (final single 90° rotation, section 4.1.4: Fig. 29), finished with BIB milling using β = 15°, V_{acc} = 3 kV, 0.5 turn osc. for 120 min, with (a) an overview and (b) a detail SEM image with an apex radius of 32 nm.

4.4.4 Proof of concept APT measurement

In contrast to the fs-laser & electropolishing section, for the process route fs-laser & BIB milling only one APT measurement was needed for a successful proof of concept. For this purpose, the specimen mentioned above (Fig. 45), prepared with β = 15°, was chosen. Starting the measurement went well, with detection of the specimen apex at around 2 kV, and reached 29 million detected ions without fracture, as depicted in Fig. 46a. The 3D reconstruction of all atoms is shown in Fig. 46b.

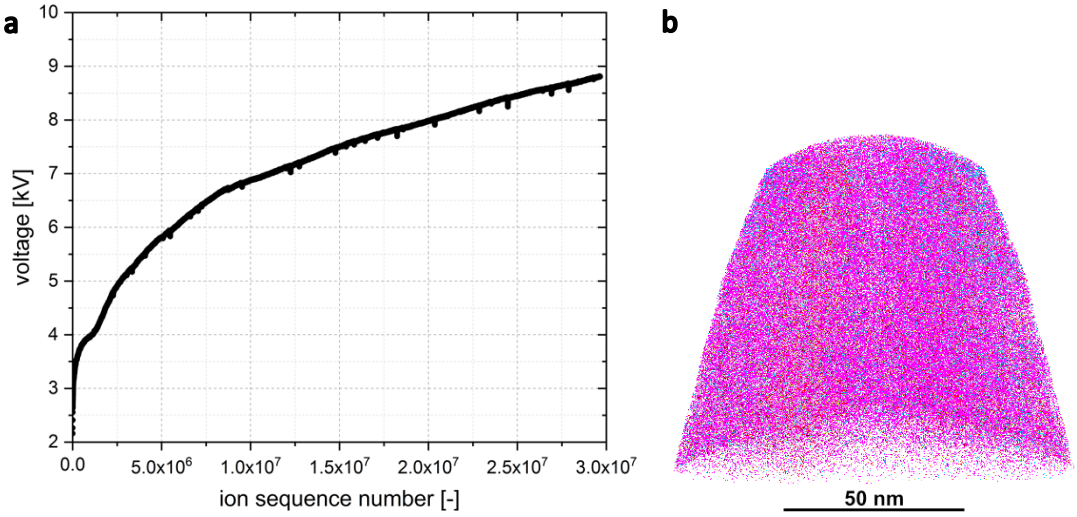

Fig. 46: Proof of concept APT measurement of the process route fs-laser & BIB milling with (a) the voltage curve and (b) the 3D reconstruction of all atoms.

Due to the higher total number of ions detected, also a reasonable visualization of different atoms/molecules in a reconstruction was possible (Fig. 47). The Ar^+ ion implantation caused by the ion BIB milling process is also shown there and has similarities to the arrangement of implanted Ga atoms during FIB preparation [33].

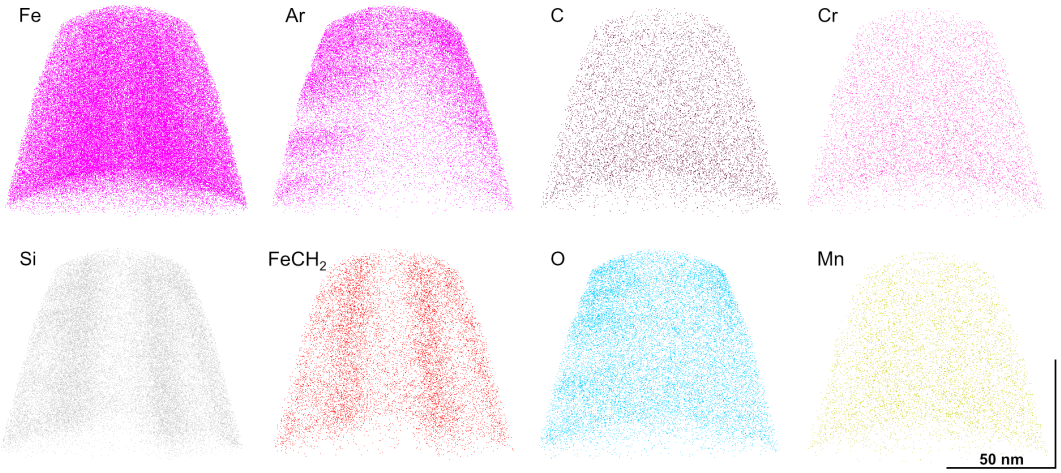

Fig. 47: 3D reconstruction from the proof of concept APT measurement of the process route fs-laser & BIB milling showing Fe, Ar, C, Cr, Si, $FeCH_2$, O and Mn.

Compared to the APT measurement of the fs-laser & electropolishing process route (section 4.1.4), the peaks could be easier differentiated from the background (30 ppm/ns). The mass spectra curve with embedded bulk decomposition is depicted in Fig. 48, with Fe as main element (98 %) and C, Si, O, Cr, Mn, Ar and Cu as accompanying elements, as well as some H as hydride.

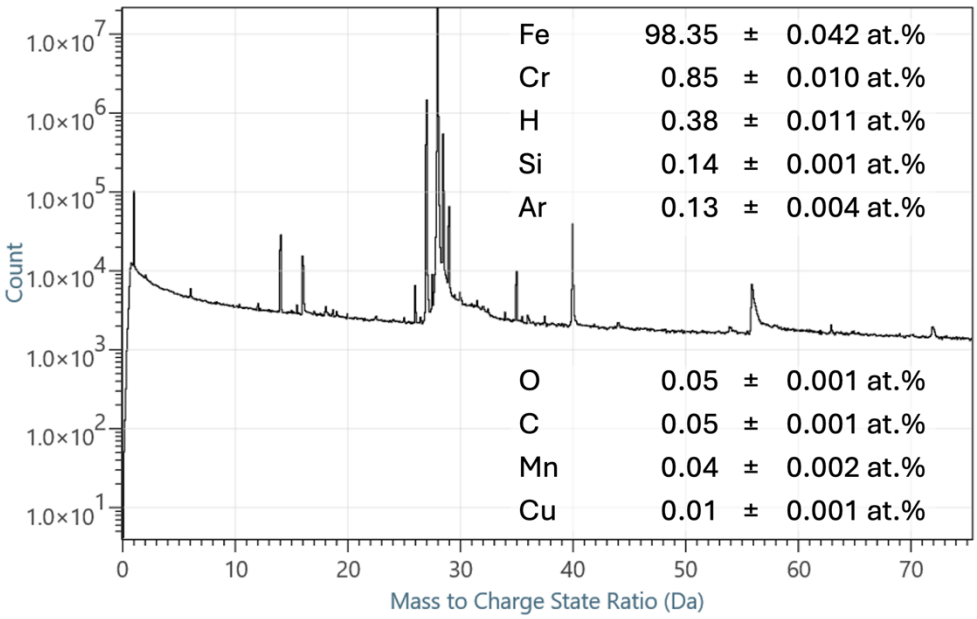

Fig. 48: Mass spectra (black line) with embedded bulk decomposition details of the proof of concept APT measurement of the process route fs-laser & BIB milling.

4.5 fs-laser & focused ion beam

4.5.1 fs-laser pre-preparation

For this whole section a fs-laser pre-prepared specimen with the rotation stage and subsequent top-down circle ablation (inner pattern diameter of 10 µm) was used. Hereby, the rotation stage preparation part was concluded with a cut using a box pattern (Fig. 49a) to create an even finish and a polygonal cross-section with about 70 µm in diameter. The top-down circle ablation laser parameters used were a power of 100 mW, the absence of a focus shift and 1001 repetitions (pattern see Fig. 49b). Despite processing with strongly reduced laser power, the ablation process was finished within 5 min, due to the small remaining cross-section.

The progress of the specimen was imaged with the built-in SEM from the FEI Versa 3D dual beam SEM/FIB workstation before, during and after the FIB preparation using 10 kV electrons. Starting directly after the fs-laser, overview SEM images are shown in Fig. 49c and in Fig. 49d with a 90° rotated specimen. This shape was similar to that of Fig. 30 (section 4.1.4), which was also rotation stage pre-prepared and finished with top-down circle ablation with an inner pattern diameter of 10 µm.

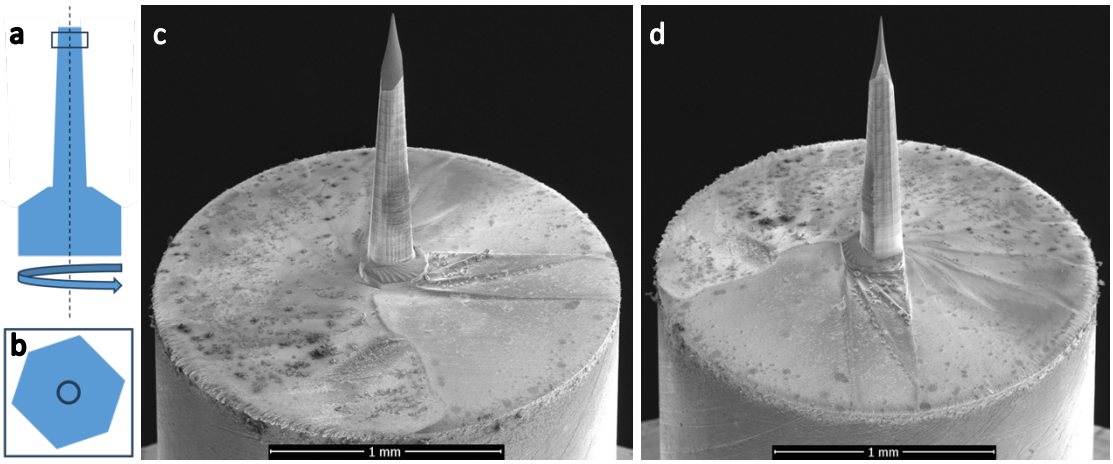

Fig. 49: fs-laser pre-prepared APT specimen using the rotation stage and subsequent top-down circle ablation (10 µm inner pattern diameter), direct before FIB preparation, with (a) the rotation stage laser pattern (b) the top-down pattern (enlarged) (c) an overview SEM image in 0° standard position and (d) 90° rotated specimen.

In the detail SEM images (Fig. 50a-d) the specimen is depicted from four different perspectives (0°, 90°, 180° and 270° rotated specimen). After the top-down circle ablation the apex was not perfectly circular, but sufficient for further FIB annular milling, far from a blade-shape (as seen at rotation stage only specimens).

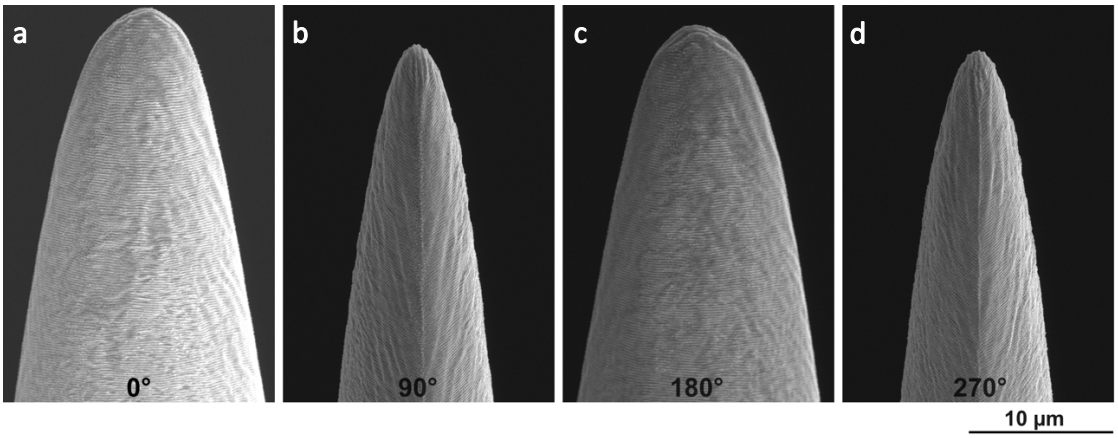

Fig. 50: Detail SEM images after the fs-laser pre-preparation using the rotation stage and top-down circle ablation (10 µm inner pattern diameter) of an APT specimen, direct before FIB preparation, with (a) 0° standard position, (b) 90°, (c) 180° and (d) 270° rotated specimen.

4.5.2 Focused ion beam annular milling

The annular milling process was performed according to section 3.4: Tab. 1 and led to the results depicted in Fig. 51. Some smaller protrusions are visible in Fig. 51a starting in a distance of approximately 2.5 µm from the primary apex and a larger protrusion on the right-hand side 10 µm away. A more detailed image of the specimen apex is shown in Fig. 51b, with a specimen radius of 54 nm.

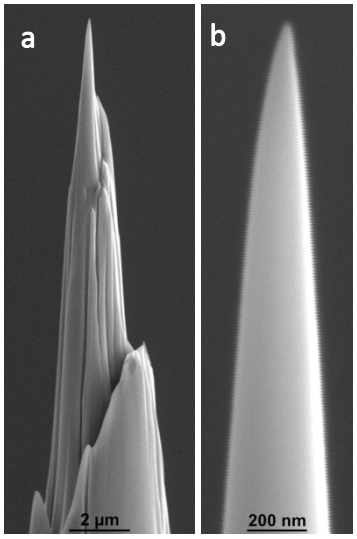

Fig. 51: Detail SEM images after FIB annular milling of an APT specimen, pre-prepared using the rotation stage and top-down circle ablation (10 µm inner pattern diameter), with (a) showing a larger area in 0° standard position and (b) a close up of the specimen apex with an apex radius of 54 nm.

4.5.3 Proof of concept APT measurement

Once again, the APT measurement started early, but was aborted fast due to specimen fracture after having reached 3.8 million detected ions, with the voltage curve shown in Fig. 52a. The 3D reconstruction of all atoms is depicted in Fig. 52b and the mass spectra curve with embedded bulk decomposition in Fig. 53, with Fe as main element and C, Si, O, Cr, Mn, Ga, Cu and Mg as accompanying elements. The peaks could easily be identified due to the low background signal (15 ppm/ns). The ion implantation of Ga^+ (0.04±0.013 at%) was caused by finishing with FIB annular milling and was lower than the Ar^+ (0.13±0.004 at%) implantation during BIB milling (from section 4.4.4).

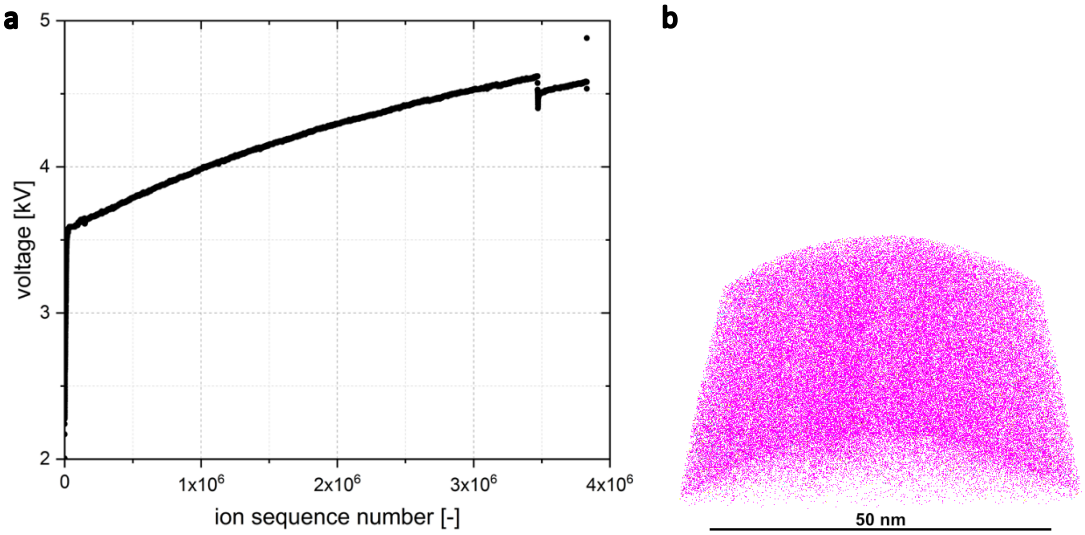

Fig. 52: Proof of concept APT measurement of the process route fs-laser & FIB annular milling, with (a) the voltage curve and (b) the 3D reconstruction of all atoms.

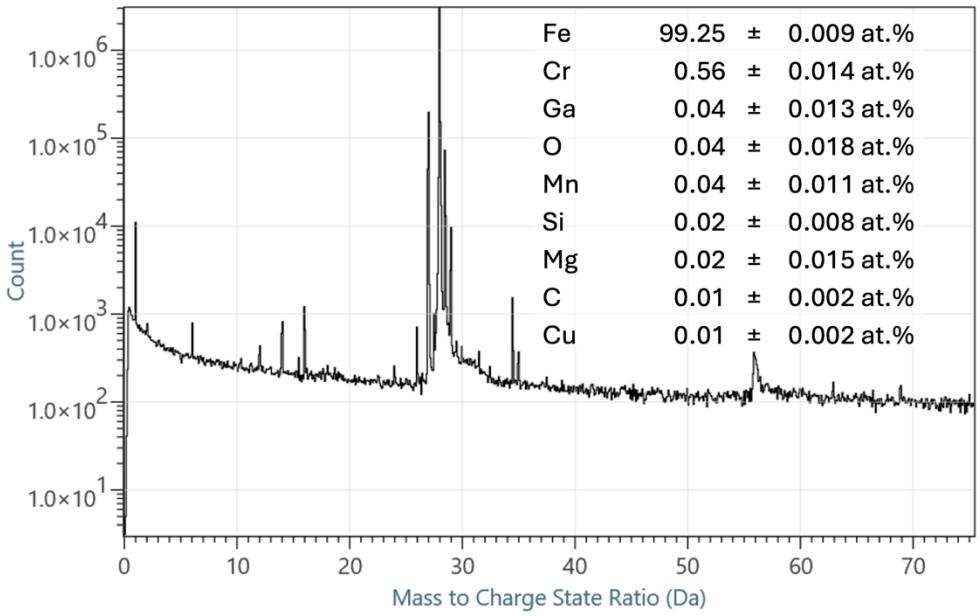

Fig. 53: Mass spectra (black line) with embedded bulk decomposition details of the proof of concept APT measurement of the process route fs-laser & FIB annular milling.

5 Summary

A femtosecond (fs)-laser ablation system was successfully implemented into all stages, except for finishing, of the preparation process of 99.5 % pure Fe atom probe tomography (APT) specimens. The three finishing processes used were either micropolishing (electropolishing step 2), broad ion beam (BIB) milling (with a low energy broad Ar^+ ion beam) or focused ion beam (FIB) annular milling. These additional steps were necessary to reach the required radius of the specimen apex in the order of 10 up to 150 nm and an appropriate shank angle for APT measurements [1,4].

Firstly, the whole rough pre-preparation, such as cutting out blanks out of a 1 mm thick sheet and cutting rods with 2 mm diameter into the desired length, was performed with this system. Hereby, increased efficiency with up to 20 pieces per process (for the sheet) and/or a first reduction of the specimen apex size (tapered shape with an end contour of 40 µm) was possible. The idea to finish those blanks directly with two-staged electropolishing was quickly discarded, due to the possibilities of the fs-laser ablation system to further decrease the specimen dimensions to be directly suitable for micropolishing. Therefore, all efforts in the fs-laser pre-preparation were made to reach a reasonably low order of magnitude in the low µm regime for further processing, with a as circular (or quadratic) shape of the specimen apex as possible.

For the fs-laser ablation experiments the laser power, pattern geometries and stage z position (to move the stage towards or away from the laser focus) was varied. Furthermore, either a standard translation (x,y-)stage (for top-down and lateral preparation direction) or a rotation stage (lateral only) was used. The convention for the laser beam direction of incidence was laser beam parallel to the specimen axis for top-down and perpendicular for lateral processes. Hereby, top-down circle ablation was the most universally applicable method, either as single process or as subsequent step after other pre-preparation routes. The resulting specimen apexes were circular shaped and reached diameters slightly below 10 µm as lower limit. If top-down ablation was used as single process, an additional step of removal of secondary apexes was necessary to ease further preparation, especially micropolishing. For lateral preparation, independent from the stage, this extra step was omitted due to the longer area, which could be prepared at once, leading to long, thin and tapered specimens. The shape of lateral thinned specimens with the x,y-stage was either quadratic with an edge length of 20 µm or higher, or square pyramidal with an end contour of only 400 nm, which turned out to be the lower limit of this system. However, the latter one only succeeded in around 50 % of the cases. The use of the rotation stage posed challenges to the centre of rotation and (even if determined correctly) led to

blade-shaped specimens. Nevertheless, with the advantage of small apex sizes of some µm and adjustable shank angles using trapezoid laser patterns. All types of fs-laser pre-prepared specimens mentioned above were investigated directly before and after further preparation (finishing with one of the three routes) using scanning electron microscopy.

Summarizing the finishing processes, for micropolishing long, thin specimens with a diameter or edge length of around 20 µm and below performed best. This was reached using either lateral thinning combined with subsequent top-down circle ablation or the rotation stage only. Hereby, the necessary necking and sharpening process lasted only 1-4 min using 8 V resulting in reproduceable apex radii of 20-70 nm. In the APT proof of concept measurements some specimens fractured early, with the best specimen resulting in 9.8 million detected ions, but at a high background level of 200 ppm/ns. In comparison, the background levels of the other APT measurements mentioned below were 15-30 ppm/ns.

In contrast to the well-known micropolishing process, the preparation parameters for APT specimens using BIB milling still had to be found. While applying 2-4 kV Ar^+ ions from an ion gun perpendicular to the specimen axis, three different tilt angles β (towards the ion gun) for the specimens were used: 15°, 35° and 60°. In general, and especially for $\beta = 35°$, the shape after BIB milling mirrored the initial shape after fs-laser ablation, a blade-shape was kept and thick round shapes as well. Blunting of the specimen apex also occurred. $\beta = 60°$ led to more efficient sharpening of the specimens, but with secondary apexes occurring and once even led to destruction of the primary apex. Experiments with $\beta = 15°$ and a fs-laser pre-prepared specimen with a shape of a square pyramid finally gave a better result: An apex radius of 31 nm without secondary apexes, but with a modest shank were achieved. This specimen was measured with APT and led to an early start of specimen apex detection at around 2 kV and 29 million detected ions with clearly distinguishable accompanying elements.

At the end, the process route fs-laser & FIB annular milling was performed with a single specimen, fs-laser pre-prepared with the rotation stage and subsequent top-down circle ablation in order to guarantee an as round as possible cross-section. The final step to reduce the apex radius from around 10 µm down to 55 nm was performed with FIB annular milling. Hereby, the proof of concept APT measurement led to 3.8 million counts before specimen fracture.

6 Outlook

In this work a fs-laser ablation system was used in as much process steps for APT specimen preparation as possible, neglecting possible alternatives. E.g., the cutting out of rectangular blanks out of a 1 mm sheet was time consuming and quickly led to necessary cleaning of the build-in filter system of the fs-laser ablation system. Reducing the sheet thickness would have decreased the cutting time significantly. Nonetheless, the large cross-section of the specimens offered advantages like no need for a Cu sleeve for APT pucks and increased mechanical stability. Furthermore, using custom shapes (individual pattern geometries) to cut details, such as tapered blanks, fs-laser processing is an advance, compared to conventional wire machining. Concerning the actual pre-preparation of APT specimen, with a cross-section of the specimen of around 200x200 μm^2 or below, the fs-laser can quickly process further. For a reduction from a larger cross-section lateral pre-thinning is worth considering. The easiest way to finish the fs-laser processing is top-down circle ablation to get a suitable dimension for either further micropolishing or FIB annular milling (if the material is difficult to electropolish). Such a single laser ablation process lasts about 5-10 min, depending on the laser power and repetitions. A laser focus shift can be used to add a longer area of constant apex diameter of the field emitter like shape. When using a blank, previously cut out of a sheet with a fs-laser custom shapes process, it should be continued with a custom shape lateral thinning process. The latter one gives a lower limit of 20 µm edge length at the specimen apex and is less suitable for FIB processing. If lower radii at the specimen apex than 8 µm are desired, the usage of a lateral preparation direction becomes inevitable. The rotation stage showed some good results for subsequent fast micropolishing, but the specimens tend to be blade-shaped, which makes them less suitable for BIB milling or FIB annular milling. Hereby, improvements concerning a stable centre of rotation are necessary. In the meantime, processing square pyramid shapes with single 90° rotation either with the x,y-stage (lateral thinning, apex radii below 1 µm are possible) or the rotation stage are an alternative for further BIB milling.

Finally, using BIB milling for finalizing fs-laser pre-prepared APT specimens a tilt angle of 15°, 3 kV acceleration voltage and 0.5 turn oscillation for the Hitachi ArBlade 5000 system is recommended. Using 120 min reduced the specimen apex size from around 5 µm to APT measurable size. Particularly worth mentioning is that the shape after BIB milling mostly mirrored the shape after fs-laser processing. Further studies investigating BIB milling different materials (apart from the used pure Fe in this work) at different tilt angles and experimental setups could further improve this outcome.

7 References

[1] A. Cerezo, P.H. Clifton, M.J. Galtrey, C.J. Humphreys, T.F. Kelly, D.J. Larson, S. Lozano-Perez, E.A. Marquis, R.A. Oliver, S.B. Gang, K. Thompson, M. Zandbergen, R.L. Alvis, Atom probe tomography today, Mater. Today 10 (2007) 12.

[2] M.K. Miller, “Atom Probe Tomography”, Springer, New York, 2000.

[3] E.W. Müller, Field Ion Microscopy, Science (1979) 149 (1965) 591–601.

[4] B. Gault, M.P. Moody, J.M. Cairney, S.P. Ringer, “Atom Probe Microscopy”, Springer, New York, 2012.

[5] M.K. Miller, K.F. Russell, G.B. Thompson, Strategies for fabricating atom probe specimens with a dual beam FIB, Ultramicroscopy 102 (2005) 287–298.

[6] D.J. Larson, T.J. Prosa, R.M. Ulfig, B.P. Geiser, T.F. Kelly, “Local Electrode Atom Probe Tomography”, Springer, New York, 2013.

[7] C. Pöhl, J. Schatte, H. Leitner, Metallographic characterization of the molybdenum based alloy MHC by a color etching technique, Mater. Charact. 77 (2013) 63–69.

[8] A. Henjered, H. Norden, A controlled specimen preparation technique for interface studies with atom-probe field-ion microscopy, J. Phys. E: Sci. Instrum. 16 (1983) 617–619.

[9] J.M. Walls, H.N. Southworth, G.J. Rushton, The preparation of field electron/field-ion emitters by ion etching, Vacuum 24 (1974) 475–479.

[10] M.K. Miller, K.F. Russell, Atom probe specimen preparation with a dual beam SEM/FIB miller, Ultramicroscopy 107 (2007) 761–766.

[11] M. Tkadletz, H. Waldl, M. Schiester, A. Lechner, G. Schusser, M. Krause, N. Schalk, Efficient preparation of microtip arrays for atom probe tomography using fs-laser processing, Ultramicroscopy 246 (2023) 113672.

[12] B. Rottwinkel, A. Kreutzer, H. Spott, M. Krause, G. Schusser, T. Höche, Preparing TEM Specimens and Atom Probe Tips by Laser Machining, Microsc. Today 27 (2019) 40–44.

[13] N. White, K. Eder, J. Byrnes, J.M. Cairney, I.E. McCarroll, Laser ablation sample preparation for atom probe tomography and transmission electron microscopy, Ultramicroscopy 220 (2021) 113161.

[14] M. Herbig, A. Kumar, Removal of hydrocarbon contamination and oxide films from atom probe specimens, Microsc. Res. Tech. 84 (2021) 291–297.

[15] E.W. Müller, J.A. Panitz, S.B. McLane, The Atom-Probe Field Ion Microscope, Rev. Sci. Instrum. 39 (1968) 83–86.

[16] T.F. Kelly, M.K. Miller, Atom probe tomography, Rev. Sci. Instrum. 78 (2007) 031101.

[17] D.J. Larson, R.M. Ulfig, D.R. Lenz, J.H. Bunton, J.D. Shepard, K.P. Rice, Y. Chen, T.J. Prosa, M. Van Dyke, N. Sridharan, S. Babu, D. Engineering Building, Microstructural Investigations in Metals Using Atom Probe Tomography with a Novel Specimen-Electrode Geometry, JOM 70 (2018) 1776–1784.

[18] M.K. Miller, R.G. Forbes, Atom probe tomography, Mater. Charact. 60 (2009) 461–469.

[19] M.A. Fortes, The shape of field-evaporated metal tips, Surf. Sci. 28 (1971) 95–116.

[20] S.T. Loi, B. Gault, S.P. Ringer, D.J. Larson, B.P. Geiser, Electrostatic simulations of a local electrode atom probe: The dependence of tomographic reconstruction parameters on specimen and microscope geometry, Ultramicroscopy 132 (2013) 107–113.

[21] D.J. Larson, K.F. Russell, M.K. Miller, Effect of Specimen Aspect Ratio on the Reconstruction of Atom Probe Tomography Data, Microsc. Microanal. 5 (1999) 930–931.

[22] K. Thompson, D. Lawrence, D.J. Larson, J.D. Olson, T.F. Kelly, B. Gorman, In situ site-specific specimen preparation for atom probe tomography, Ultramicroscopy 107 (2007) 131–139.

[23] M.K. Miller, K.F. Russell, G.B. Thompson, Strategies for fabricating atom probe specimens with a dual beam FIB, Ultramicroscopy 102 (2005) 287–298.

[24] M. Tkadletz, A. Lechner, S. Pölzl, N. Schalk, Anisotropic wet-chemical etching for preparation of freestanding films on Si substrates for atom probe tomography: A simple yet effective approach, Ultramicroscopy 230 (2021) 113402.

[25] S. Hestad, F. Pérez-Willard, C. Hartfield, K. Crosby, R. Ulfig, K. Rice, Laser Ablation: A New Approach to APT Specimen Preparation, Microsc. Microanal. 28 (2022) 50–51.

[26] M. Heller, V. Schon, B. Ott, P. Felfer, Laser Ablation Sample Preparation for Grain Boundary Analysis of H in Atom Probe Tomography, Microsc. Microanal. 28 (2022) 694–696.

[27] P. Deepu, T. Jagadesh, D. Muthukannan, B. Jagadeesh, Investigation into femtosecond based laser ablation and morphology of micro-hole in titanium alloy, Optik 274 (2023) 170519.

[28] D. Ruthe, K. Zimmer, T. Höche, Etching of CuInSe 2 thin films - Comparison of femtosecond and picosecond laser ablation, Appl. Surf. Sci. 247 (2005) 447–452.

[29] J.G. Gigax, H. Vo, Q. McCulloch, M. Chancey, Y. Wang, S.A. Maloy, N. Li, P. Hosemann, Micropillar compression response of femtosecond laser-cut single crystal Cu and proton irradiated Cu, Scr. Mater. 170 (2019) 145–149.

[30] T.L. Burnett, R. Kelley, B. Winiarski, L. Contreras, M. Daly, A. Gholinia, M.G. Burke, P.J. Withers, Large volume serial section tomography by Xe Plasma FIB dual beam microscopy, Ultramicroscopy 161 (2016) 119–129.

[31] D.J. Larson, K.F. Russell, A. Cerezo, Sharpening of field-ion specimens and positioning of features of interest by ion-beam milling, J. Vac. Sci. Technol. 18 (2000) 328–333.

[32] T. Sato, Y. Aizawa, H. Matsumoto, M. Kiyohara, C. Kamiya, F. von Cube, Low damage lamella preparation of metallic materials by FIB processing with low acceleration voltage and a low incident angle Ar ion milling finish, J. Microsc. 279 (2020) 234–241.

[33] K. Thompson, D. Lawrence, D.J. Larson, J.D. Olson, T.F. Kelly, B. Gorman, In situ site-specific specimen preparation for atom probe tomography, Ultramicroscopy 107 (2007) 131–139.